ments. One patient (one ankle) died for reasons unrelated to the operation. Four patients (four ankles) were lost to follow-up at the time of review. The remaining 27 ankles in 21 patients were evaluated. Average patient age at the time of surgery was 60 (36–75) years, and average follow-up was 72 (15–169) months. Twenty patients had other lower extremity joint replacements. In all patients, the major complaint before surgery was pain and disability in walking.

The implant used was the TNK ankle (Kyocera, Kyoto, Japan), which is made of ceramic and ultra-high-molecular-weight polyethylene [13]. A ceramic implant, provided with a medial facet joint, was inserted from the anterior side. Three sizes (small, medium, and large) were available. The operation was done using an anterior approach as described previously [13]. With the patient under general anesthesia, implants were anchored with cement. A tourniquet was used to control bleeding during surgery.

A longitudinal incision was made between the tibialis anterior tendon and the extensor hallucis longus tendon to retract laterally the dorsalis pedis artery and deep peroneal nerve. Synovium in the tendon sheath of the extensor tendons and at the lateral and medial facet in the joint were removed. The cutting guide for the tibial osteotomy was inserted, and the osteotomy was done from an anterior opening at an angle of 80° from the long axis of the tibia and exited from the posterior tibial cortex. A talar osteotomy was done according to the cutting guide. An anchor hole in the talus was made according to the guide, the trial implant was inserted, and alignment and mobility were examined. The implants were fixed with cement, and a suction drain was inserted followed by suturing. A short leg cast was applied with the ankle in slightly dorsiflexed position. The suction drain was removed 48 h postoperatively. A short leg cast was maintained for 3 weeks before beginning ankle motion to allow for soft-tissue healing. Active flexion-extension began after cast removal. Weight bearing began 4 weeks after the operation.

Clinical results, range of motion (ROM), questionnaires, radiographic findings, complications, and survival rate were examined. Clinical results were evaluated using the clinical rating scale of the American Orthopaedic Foot and Ankle Society (AOFAS) (100 points total) [5]. The questionnaire assessed the level of pain, function, and alignment. Patients were asked to rate pain on a scale of 0–40 points. Function was calculated as the total score of activity limitations (0–10), maximum walking distance (0–5), walking surface (0–5), gait abnormality (0–8), sagittal motion (0–8), hindfoot motion (0–6), and ankle-hindfoot stability (0–8). Alignment was rated from 0 to 10 points (good, fair, poor), giving a total score of 100 points. Excellent was defined as a score of 85–100, good as 75–84, fair as 70–74, and poor as less than 70.

At the latest follow-up questionnaires were completed by 17 patients (24 ankles) whose implants had survived. The questionnaire assessed preoperative and postoperative condition, degrees of satisfaction with the operation, and complaints. Radiolucent lines at the interface between the component and the bone were assessed on anteroposterior (AP) and lateral radiographs. Tibial component migration and talus collapse were also examined. Survival rate was calculated using the Kaplan-Meier method at revision surgery as the end point.

Results

Pain relief was the primary criterion of success in this study. The implant in three patients (three ankles) had been removed because of pain and component loosening. One ankle was treated with revision total ankle replacement, and two ankles were treated with arthrodesis. At the latest follow-up of the 24 surviving ankles in 17 patients, the average ankle-hindfoot score was 66.3 (32–90) points. Clinical results were graded excellent in two ankles, good in seven, fair in three, and poor in 12 (Table 1). Average pain score was 33 (0–40) points. Eleven patients with 13 ankles had no pain. Plantar flexion was 8.5° (−10–20°) and dorsiflexion was 7.5° (0–20°). Average scores for sagittal motion was 3 (0–8) points and hindfoot motion 0 points.

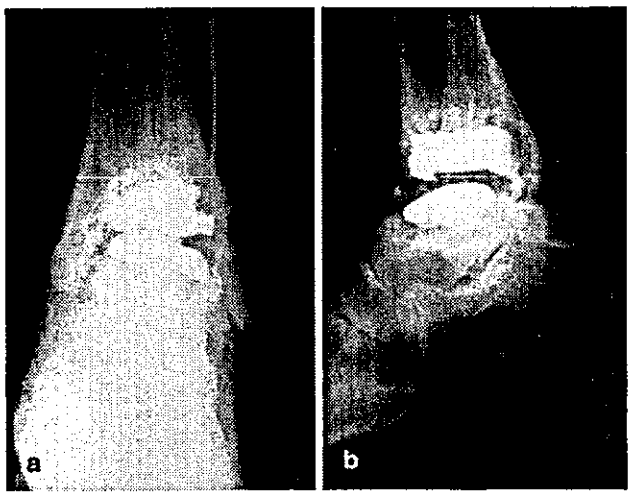

Fig. 1 **a** Anteroposterior radiograph showing migration of the tibial component. **b** Lateral radiograph showing collapse of talus after TNK arthroplasty

Table 1 Average American Orthopaedic Foot and Ankle Society (AOFAS) ankle-hindfoot score at latest follow-up. Total score: 66.3 (range 32–90)

Pain	Function	Walking distance
33.0	4.3	3.3
Walking surface	Gait abnormality	Sagittal motion
2.6	4.7	3.0
Hindfoot motion	Ankle-hindfoot stability	Alignment
0	8.0	7.3

Questionnaires were sent to 17 patients whose implants survived until follow-up, with 15 questionnaires (21 ankles) returned. Conditions compared with before surgery mostly had improved. Twelve patients with 16 ankles improved, and one patient with two ankles deteriorated. Five patients with seven ankles were extremely satisfied, and six patients with eight ankles were satisfied. Major complaints included deformity, low mobility, and pain.

On anteroposterior radiographs, 18 ankles had radiolucent lines at the tibial component and nine also radiolucent lines at the talar component. On lateral radiographs, 15 ankles had radiolucent lines at the tibial component and 12 also had radiolucent lines at the talar components. Tibial component migration was seen in 13 ankles, and talus collapse was seen in nine (Fig. 1a,b).

Complications involved loosening in 10 ankles. One ankle was treated with revision total ankle replacement; however, the ankle later was fused because of early loosening 2 years after revision surgery. Two ankles were treated with arthrodesis. However, two of three fused

ankles fractured within 1 year after arthrodesis and required additional surgery. The remaining seven ankles had mild symptoms, and therefore were followed up without additional therapy. Delayed wound healing occurred in one ankle, which eventually healed with conservative therapy without any deep infection. Intraoperative fracture of the medial facet occurred in one ankle and was treated with internal fixation. Survival rate was 77% at 169 months using revision surgery as the end point.

Discussion

The results of total ankle replacement are not always as satisfactory as total hip replacement or total knee replacement. Many authors recommend ankle arthrodesis for ankle end-stage arthritis as the primary surgical treatment. Dini et al. [3] reported that of 21 Smith total ankle replacements, only 50% were rated as good at the 3-year follow-up. Kitaoka et al. [4] also reported poor results of 204 Mayo-type, total ankle replacements at the 9-year follow-up and stated that "we no longer recommend ankle arthroplasty." Bolton-Maggs et al. [1] reported the results of 62 total ankle replacements after 5.5 years' follow-up and reported only 13 ankles that could be described as satisfactory. Takakura et al. [13] reported the results 69 TNK total ankle replacements with satisfactory results (excellent, good) in only 24% of ankles with a cemented metal component.

Although these reports included both patients with osteoarthritis and patients with rheumatoid arthritis, only patients with rheumatoid arthritis were evaluated in the current study. Only Lachiewicz et al. [6] have reported the results of total ankle replacement in patients with rheumatoid arthritis. Of 15 total ankle arthroplasties in patients with rheumatoid arthritis at 39 months follow-up, seven were rated as excellent and eight as good. Pain relief was gratifying in all their patients. They reported that moderate-to-severe arthritic changes were present in other tarsal joints, and no inversion or eversion motion was observed in many patients. They reported total ankle replacement could be successful in carefully selected patients with severe arthritis of the ankle.

The analysis of old total ankle replacements indicated that the major factors of failure are the fixation method and component design. Takakura et al. [13] reported that uncemented ceramic components with less bone resection yield better results than cemented metal components. The many early design components usually were highly constrained. The high rates of constrained implant loosening are thought to be from greater stress at the bone-prosthesis interface, as constrained implants do not allow rotation and sliding during extension and flexion.

Cement fixation was used for all patients in the current study despite the fact that other authors have shown that uncemented ceramic components with less bone resection yield better results than cemented metal components [12, 13]. The reason for this decision was that patients with rheumatoid arthritis in the current study had severe osteoporosis develop after using corticosteroids for long periods [10], rendering the use of uncemented fixation too problematic in many patients.

If component loosening occurs, revision surgery or arthrodesis is required. However, this operation is difficult to do because of massive bone loss and poor bone quality. In the current study, one patient (one ankle) had revision total ankle replacement; however, reloosening occurred in 2 years. The ankle then was treated by arthrodesis but fractured after 8 months, requiring additional surgery. The average ROM at the follow-up was approximately 15°. This range is not satisfactory because of the implant design.

Patients with rheumatoid arthritis often have several joint deformities in the lower extremities by the time the ankle is surgically treated. In the current study, all patients except one already had other joint replacements in their lower extremities when the total ankle replacement was done, which may explain the poor clinical score. Patients with no pain cannot live highly active lives because of severe deformities from rheumatoid arthritis requiring multiple operations.

Radiographs showed radiolucent lines around components, implant migration, and talus collapse; however, unacceptable residual pain was observed in only a few patients. Patients with a low clinical score, or loosening or sinking of components, do not always experience pain. Sixty percent of patients with poor results were satisfied, and none was disappointed.

Patients with rheumatoid arthritis usually have degeneration of subtalar and midtarsal joints and no inversion or eversion motion of the ankle by the time they need surgery. If arthrodesis is done in those ankles, increased stress affects other joints and worsens functions such as gait. Although the results of total ankle replacement are poor, the degree of patient satisfaction is not poor in those with rheumatoid arthritis. Therefore, total ankle replacement is an important therapy that can retain hindfoot motion for patients with rheumatoid arthritis.

The latest component design is semiconstrained to allow for rotation and sliding during extension and flexion. Reports of the agility total ankle system (two-component) [11] and the STAR total ankle system (mobile bearing) were encouraging [12]. Future improvements of component design, fixation method, and surgical technique are required to improve outcomes.

The results of 27 total ankle arthroplasties in 21 patients with rheumatoid arthritis were evaluated. Residual pain was present in 11 ankles, with radiographs showing a high incidence of radiolucent lines. There were 13 tibial component migrations and nine talus collapses at follow-up. For low hindfoot mobility in patients with rheumatoid arthritis, total ankle replacement that can retain ankle function is an important therapeutic option; however, implant designs and surgical methods that produce stable results need to be developed.

References

1. Bolton-Maggs BG, Sudlow RA, Freeman MAR (1985) Total ankle arthroplasty: A long-term review of the London hospital experience. J Bone Joint Surg [Br] 67:785–790
2. Dereymaeker GP, Eygen PV, Driesen R, Ferm AD (1998) Tibiotalar arthrodesis in the rheumatoid foot. Clin Orthop 349:43–47
3. Dini AA, Bassett FH (1980) Evaluation of the early result of Smith total ankle replacement. Clin Orthop 146:228–230
4. Kitaoka HB, Patzer GL (1996) Clinical results of the Mayo total ankle arthroplasty. J Bone Joint Surg [Am] 78:1658–1664
5. Kitaoka HB, Alexander IJ, Adelaar RS, Adelaar RS, Nunley JA, Myerson MS, Sanders M (1994) Clinical rating systems for the ankle-hindfoot, midfoot, hallux, and lesser toes. Foot Ankle Int 15:349–353
6. Lachiewicz PF, Inglis AE, Ranawat CS (1984) Total ankle replacement in rheumatoid arthritis. J Bone Joint Surg [Am] 66:340–343
7. Lance EM, Pavel A, Patterson RL Jr , Fries I, Larsen IJ (1971) Arthrodesis of the ankle: A follow-up study. J Bone Joint Surg 53:1030
8. Mazur JM, Schwartz E, Simon SR (1979) Ankle arthrodesis: Long-term follow-up with gait analysis. J Bone Joint Surg [Am] 61:964–975
9. Miehlke W, Gschwend N, Rippstein P, Simmen BR(1997) Compression arthrodesis of the rheumatoid ankle and hindfoot. Clin Orthop 340:75–86
10. Newton SE III (1982) Total ankle arthroplasty: Clinical study of fifty cases. J Bone Joint Surg [Am] 64:104–111
11. Pyevich MT, Saltzman CL, Callaghan JJ, Alvine FG (1998) Total ankle arthroplasty: A unique design: Two-to-twelve-year follow-up. J Bone Joint Surg [Am] 80:1410–1420
12. Saltzman CL, Mclff TE, Buckwalter JA, Brown TD (2000) Total ankle replacement revised. J Orthop Sports Phys Ther 30:56–67
13. Takakura Y, Tanaka Y, Sugimoto K, Tamai S, Masuhara K (1990) Ankle arthroplasty: A comparative study of cemented metal and uncemented ceramic prostheses. Clin Orthop 252:209–216

J Bone Miner Metab (2004) 22:176–184
DOI 10.1007/s00774-003-0468-9

Journal of
Bone and
Mineral
Metabolism

Original articles

Matrix extracellular phosphoglycoprotein (MEPE) is highly expressed in osteocytes in human bone

Akihide Nampei[1], Jun Hashimoto[1], Kenji Hayashida[1], Hideki Tsuboi[1], Kenrin Shi[1], Isamu Tsuji[4], Hideaki Miyashita[4], Takao Yamada[4], Naomichi Matsukawa[2], Masayuki Matsumoto[3], Shigeto Morimoto[3], Toshio Ogihara[2], Takahiro Ochi[1], and Hideki Yoshikawa[1]

[1]Department of Orthopaedics, Osaka University Graduate School of Medicine, 2-2 Yamadaoka, Suita 565-0871, Japan
[2]Department of Geriatric Medicine, Osaka University Graduate School of Medicine, Osaka, Japan
[3]Department of Geriatric Medicine, Kanazawa Medical University, Kanazawa, Japan
[4]Pharmaceutical Research Division, Takeda Chemical Industries, Osaka, Japan

Abstract The matrix extracellular phosphoglycoprotein (MEPE) gene is highly expressed in tumors that cause oncogenic hypophosphatemic osteomalacia (OHO). MEPE is also known as one of the bone-tooth matrix proteins and is associated with bone mineralization. We developed a rabbit polyclonal antibody directed against recombinant human MEPE (rhMEPE) after cloning its cDNA from the cDNA library of a nasal tumor tissue causing OHO. Using this antibody, we analyzed the distribution of MEPE in human bones by immunohistochemistry. In bone specimens from normal subjects, MEPE was predominantly expressed by osteocytes and not by osteoblasts. In bone specimens from patients with osteomalacia, however, MEPE was focally expressed by deeply located osteocytes. We also compared the MEPE positivity of osteocytes in mineralized bone and non-mineralized osteoid obtained from patients with osteomalacia and osteoporosis. Among osteomalacia patients, MEPE positivity was seen in 87.5 ± 8.6% of the osteocytes from mineralized bone compared with 7.8 ± 6.4% of those from osteoid. Among osteoporosis patients, MEPE positivity was found in 95.3 ± 0.5% of the osteocytes from mineralized bone compared with 4.9 ± 5.7% of those from osteoid. MEPE was mainly expressed by osteocytes embedded in the matrix of mineralized bone from patients with osteomalacia or osteoporosis. Our data provide the first histological evidence that MEPE is predominantly expressed by osteocytes in human bone, with significant expression by osteocytes within mineralized bone.

Key words MEPE · osteocyte · immunohistochemistry · mineralization · human

Introduction

Matrix extracellular phosphoglycoprotein (MEPE) is a glycosylated protein that was originally cloned from the tumors of patients with oncogenic hypophosphatemic osteomalacia (OHO) [1]. Because of its high expression in tumors that cause OHO, MEPE is regarded as a candidate phosphatonin, a putative humoral factor causing hypophosphatemic osteomalacia [2]. The MEPE gene has similarities with the genes of bone-tooth mineral matrix phosphoglycoproteins called SIBLINGs (small integrin-binding ligand with N-linked glycosylation) which contain RGD sequences that have been proposed as essential for integrin-receptor interactions [3]. This group of proteins includes osteopontin (OPN), dentin sialo phosphoprotein (DSPP), dentin matrix protein 1 (DMP1), and bone sialo protein (BSP).

MEPE also appears to be associated with the mineralization of bone. Petersen et al. [4] reported that osteoblast/osteocyte factor 45 (OF 45), which is identical to MEPE, was specifically expressed in bone tissue and that its expression was increased during matrix mineralization mediated by rat bone marrow-derived osteoblasts. They also showed that this protein was highly expressed by osteocytes embedded within the bone matrix. Argiro et al. [5] reported that murine MEPE mRNA was expressed by fully differentiated osteoblasts in vitro and that its expression was markedly increased during murine osteoblast-mediated matrix mineralization in normal and Hyp mice. Recently, Gowen et al. [6] reported that OF 45 knockout mice showed an increase in bone mass due to an increase in osteoblast numbers and activity. These findings suggest that MEPE may have a direct influence on bone metabolism, not only on renal phosphate handling but also on the mineralization of osteoid.

Although MEPE expression at the protein level has been demonstrated in mice [6] and rats [4], MEPE expression in human bone remains unproven. We developed a rabbit polyclonal antibody directed against recombinant human (rh)MEPE, which was obtained by the expression of MEPE cDNA in *Escherichia coli*. In

Offprint requests to: J. Hashimoto
(e-mail: junha@ort.med.osaka-u.ac.jp)
Received: May 23, 2003 / Accepted: September 12, 2003

this study, we demonstrated the expression of MEPE histologically in bone tissue from normal subjects, patients with several types of osteomalacia (OHO, Fanconi's syndrome, and vitamin D-deficient rickets), and patients with osteoporosis.

Subjects, materials, and methods

Preparation of polyclonal anti-MEPE antibody

We constructed a cDNA library from the nasal tumor of a patient with OHO [7], and cloned human MEPE cDNA using primers designed from the reported MEPE DNA sequence [1]. Then we obtained rhMEPE by expression in *E. coli* and developed a rabbit polyclonal antibody against rhMEPE. Briefly, a rabbit was immunized with rhMEPE (1 mg) in Freund's complete adjuvant (Wako, Osaka, Japan) injected at multiple subcutaneous sites on the back and intramuscularly into both thighs. After 2, 4, 6, and 8 weeks, the rabbit was given a half dose (0.5 mg) of rhMEPE in Freund's incomplete adjuvant (Wako). One week after the final booster injection, the rabbit was killed to obtain 70 ml of antiserum. The anti-serum had a titer of around 10^6–10^7 when assayed by enzyme immunoassay (EIA), using horseradish peroxidase (HRP)-conjugated anti-rabbit IgG (Wako). The anti-serum (6 ml) was diluted twofold with MAPSII binding buffer (Bio-Rad Laboratories, Tokyo, Japan), and applied to a column of Protein A-Sepharose FF (1.6 × 5.0 cm, 10 ml; Amersham Biosciences, Tokyo, Japan). An IgG fraction was eluted from the column with MAPSII elution buffer (Bio-Rad Laboratories), followed by neutralization. After dialysis against phosphate-buffered saline (PBS), the IgG fraction was chromatographed on a column of MEPE-coupled NHS-Hitrap (1 ml, containing 3 mg of coupled rhMEPE; Amersham Biosciences). The specific antibody fraction was eluted with 0.5 M NaCl–0.1 M glycine-HCl (pH 2.7). After neutralization and dialysis against PBS, the affinity-purified anti-MEPE IgG fraction was stored at 4°C until use. Starting from 6 ml of anti-serum, 16 mg of rabbit polyclonal anti-MEPE antibody was obtained. To confirm the specificity of this anti-rhMEPE antibody, a Western blot was performed of a crude cell lysate of *E. coli* expressing rhMEPE, using anti-MEPE IgG and HRP-conjugated goat anti-rabbit IgG (Wako) as the primary and secondary antibodies, respectively. To confirm the detectability of rhMEPE expressed by a mammalian host, immunoblotting with the anti-MEPE antibody of the culture medium of rhMEPE-transfected Chinese hamster ovary (CHO) cells was also performed.

Clinical profile of the subjects

Samples of normal bone tissue were obtained intraoperatively from two patients: intact bone was obtained from a site away from a traumatic fracture of the tibia in a healthy 18-year-old man (NC1), and intact fibula was obtained from a 2-year-old boy who underwent below-knee amputation for fibrosarcoma of the tibia (NC2). Informed consent was obtained in both cases.

Iliac bone samples affected by osteomalacia (OM1-4; $n = 4$) and osteoporosis (OP1-4; $n = 4$) were obtained from patients who were diagnosed on the basis of bone mineral density, laboratory data, and iliac bone biopsy findings. Of the patients with osteomalacia, two had OHO (OM1, 2), one had Fanconi's syndrome (OM3), and one had vitamin D-deficient rickets (OM4). The clinical characteristics of all patients are summarized in Table 1.

Preparation of specimens

Paraffin sections

Decalcified paraffin sections were prepared for immunohistochemistry to detect MEPE. Bone samples from NC1, NC2, and OM1 were fixed in 4% paraformaldehyde (pH 7.4) at 4°C for 24 h, decalcified in 20% ethylenediamine tetraacetic acid (EDTA) (pH 7.4), dehydrated through an ethanol series, and finally embedded in paraffin. The specimens were then cut into serial sections (5-μm-thick) on a microtome, mounted on slides, and prepared for immunohistochemistry. One of the sections was stained with hematoxylin and eosin to assess the histological features of each bone specimen.

Methylmethacrylate (MMA) sections

Sections were also prepared from undecalcified tissue to distinguish between the calcified and noncalcified areas. Iliac bone samples from the four osteomalacia patients (OM1-4) and the four osteoporosis patients (OP1-4) were fixed in 70% ethanol, prestained with Villanueva bone stain for 7 days, dehydrated through an ethanol and acetone series, and embedded in MMA, as described [8]. To distinguish noncalcified osteoid as Villanueva-positive areas, dry sections (5-μm-thick) were cut, using a Jung Supercut 2065 Microtome (Leica Microsystems, Heidelberg, Germany) equipped with a tungsten carbide knife. For immunohistochemistry, serial wet sections (5-μm-thick) were cut with the same machine while applying 30% ethanol to the block and knife. These sections were carefully stretched using 70% ethanol, mounted on gelatin-coated slides, using a mixture of carbolic acid crystals and glycerol, flattened with a rubber roller, pressed with a slide press, and dried on a hot plate at 40°C.

Table 1. Characteristics of patients

Patient	Age (years)	Sex	Diagnosis	Bone histomorphometric data			Serum data					
				OS/BS (%)	O.Th (μm)	MAR (μm/day)	Calcium (8.4–10.0 mg/dl)	Phosphorous (2.9–4.8 mg/dl)	ALP (69–135 IU/l)	1,25(OH)$_2$vitD (20–60 pg/ml)	25(OH)vitD (10–55 pg/ml)
NC1	18	M	Tibial fracture	NA	NA	NA	NA	NA	NA	NA	NA
NC2	2	M	Amputation	NA	NA	NA	NA	NA	NA	NA	NA
OM1	53	F	Oncogenic osteomalacia	83.6	42.8	CND	8.5	1.8	356	12.5	NA
OM2	58	F	Oncogenic osteomalacia	80.1	38.0	CND	8.0	1.6	472	18.0	29
OM3	35	F	Fanconi's syndrome	90.2	50.0	CND	8.2	2.4	947	9.2	24
OM4	53	F	Vitamin D deficiency	97.3	117.5	CND	7.1	2.4	264	23.5	16
OP1	53	M	Osteoporosis	16.7	10.2	0.78	8.3	4.6	118	61.3	6
OP2	54	F	Osteoporosis	20.2	9.4	NM	8.9	4.6	101	61.7	21
OP3	65	M	Osteoporosis	12.1	13.1	0.66	9.8	3.6	147	67.4	25
OP4	45	F	Osteoporosis	20.2	9.4	0.61	9.4	4.9	99	66.0	NA

OS/BS, osteoid surface/bone surface; O.Th, osteoid thickness; MAR, mineral apposition rate; CND, calculation not done; NM, no measurement; NA, not available; NC, normal control; OM, osteomalacia; OP, osteoporosis

Immunohistochemical staining

Paraffin-embedded tissue sections were deparaffinized, and MMA-embedded sections were deacrylated twice in acetone, for 8 min each time, and then decalcified in 20% EDTA (pH 7.4) for 1 h. After being rinsed with water for 10 min, the sections were incubated in 0.3% H_2O_2 in 90% methanol for 30 min at room temperature to block endogenous peroxidase activity, and then the sections were incubated in 10% normal goat serum to minimize nonspecific background staining. Next, the rabbit polyclonal antibody directed against human MEPE was applied to each section, followed by incubation overnight at 4°C. An isotype-matched IgG was used for control staining. Detection was then performed using the streptavidin biotin-peroxidase complex technique (Histofine SAB-PO Kit; Nichirei, Tokyo, Japan) before the sections were developed in 3,3′-diaminobenzidine tetrahydrochloride (Dojindo Laboratories, Kumamoto, Japan) and counterstained with hematoxylin.

Analysis of MEPE expression by osteocytes

MEPE expression by osteocytes was analyzed in mineralized bone and non-mineralized osteoid from all bone samples. Sections immunostained for MEPE, as well as Villanueva-stained MMA-embedded sections, were examined under a light microscope (ECLIPSE E1000; Nikon, Tokyo, Japan). Five randomly chosen visual fields within the trabecular bone area were examined at 200× magnification. The number of osteocytes was counted in the mineralized and non-mineralized areas of the Villanueva-stained section. Then the number of MEPE-positive cells was counted in the immunostained serial section in the areas that corresponded to those characterized as mineralized or non-mineralized by Villanueva staining. Subsequently, the ratio of MEPE-positive osteocytes to the total number of osteocytes in the mineralized bone and the non-mineralized osteoid was calculated. Values for results are presented as means ± SDs. Statistical analysis was performed using the Mann-Whitney U-test, and statistical significance was established at the $P < 0.05$ level.

Results

Western blotting of rhMEPE using the anti-MEPE polyclonal antibody

The specificity of the anti-MEPE antibody was examined by the Western blotting of both a crude lysate of *E. coli* expressing rhMEPE and of the culture medium of CHO cells transfected with a MEPE expression plasmid (Fig. 1). When the *E. coli* lysate was tested, rhMEPE

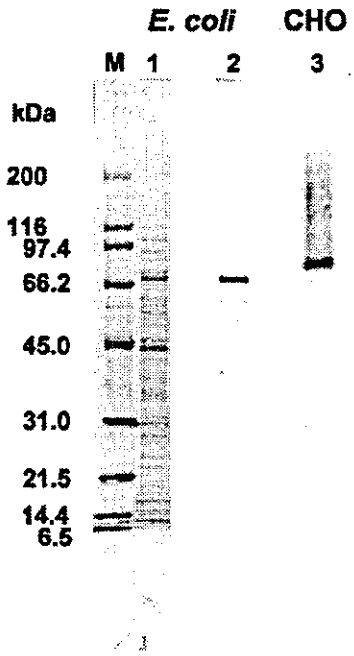

Fig. 1. Western blot analysis of recombinant human matrix extracellular phosphoglycoprotein (rhMEPE) expressed in *Escherichia coli* and Chinese hamster ovary (*CHO*) cells. A cell lysate prepared from *E. coli* expressing rhMEPE was stained with Coomassie Blue (*lane M*, molecular weight markers; *lane 1*, the *E. coli* lysate) and the lysate was also immunostained (*lane 2*) with anti-MEPE antibody. Culture medium from CHO cells transiently expressing rhMEPE was also analyzed by Western blotting (*lane 3*)

immunoreactivity was visualized as a single band at 67 kDa (lane 2; Fig. 1), demonstrating high specificity of the anti-MEPE antibody. When CHO cells were tested, a secreted protein of 70 kDa was selectively detected (lane 3; Fig. 1), confirming the specificity of the antibody. A broad, faint band was also observed at 100–150 kDa, indicating the secretion of heavily glycosylated forms of MEPE by the CHO transfectants.

Uniform MEPE expression in normal bone

MEPE expression was examined in normal bone tissue. Figure 2 shows MEPE expression in adult bone (NC1, tibial fracture), and Fig. 3 shows its expression in bone from a child (NC2, intact fibula). MEPE was strongly expressed by osteocytes in both cortical bone and trabecular bone (Fig. 2B, F), but it was not expressed by osteoblasts (Fig. 3C). Strong MEPE expression was observed in dendritic processes, as well as in the pericellular bone matrix of these bone-embedded osteocytes (Fig. 2D, H).

Focal MEPE expression in bone from osteomalacia patients

Bone specimens from osteomalacia patients were also examined. Figure 4 shows the bone specimen from a patient with OHO (OM1). MEPE expression was predominant in the osteocytes of cortical bone, although focal expression was also seen in trabecular bone (Fig. 4B); expression was more abundant in the central area

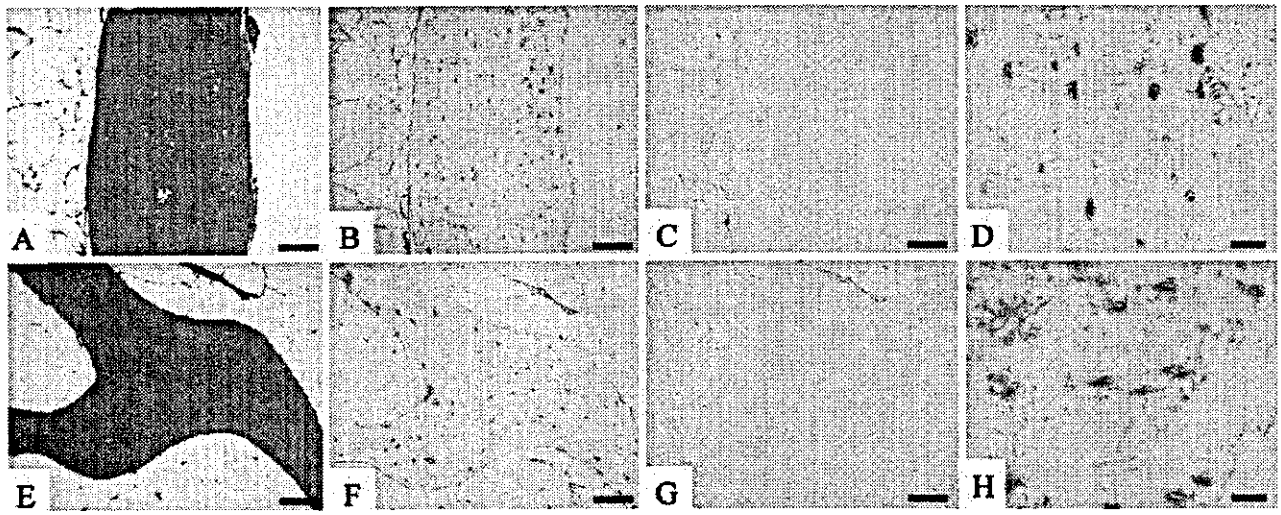

Fig. 2. Immunohistochemical detection of MEPE in normal human bone tissue (subject, NC1); **A–D** cortical bone; **E–H** trabecular bone from the tibia. **A,E** Staining with H&E. **B,D, F,H** Immunolocalization of MEPE; **C,G** negative control, and **D,H** higher magnifications of **B** and **F**, respectively. **B,F** MEPE is uniformly expressed by osteocytes embedded in the matrix of both cortical and trabecular bone. **D,H** The dendritic processes and pericellular bone matrix of osteocytes are also positive. *Bar*, 100 μm in **A–C** and **E–G**; *bar*, 20 μm in **D** and **H**

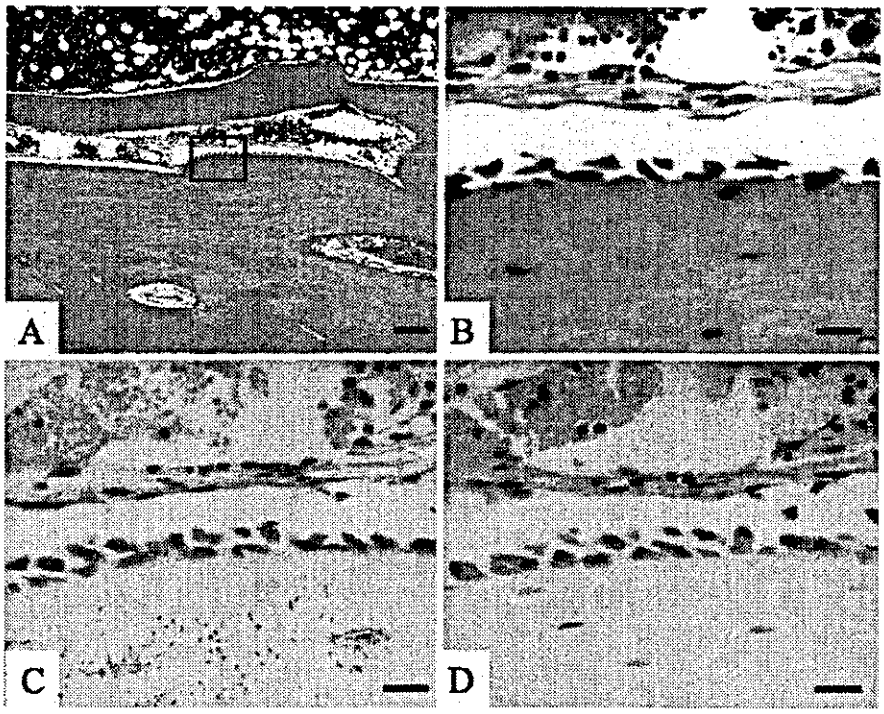

Fig. 3. Immunohistochemical detection of MEPE in immature bone (subject, NC2); **A, B** H&E staining; **C** anti-MEPE antibody; **D** negative control. **B** Higher magnification of the *boxed area in A*. **C** Osteoblasts are not stained, but osteocytes, pericellular bone matrix, and dendritic processes are stained, as was the case in mature bone (Fig. 2). *Bar*, 150 μm in **A**; *bar*, 20 μm in **B–D**

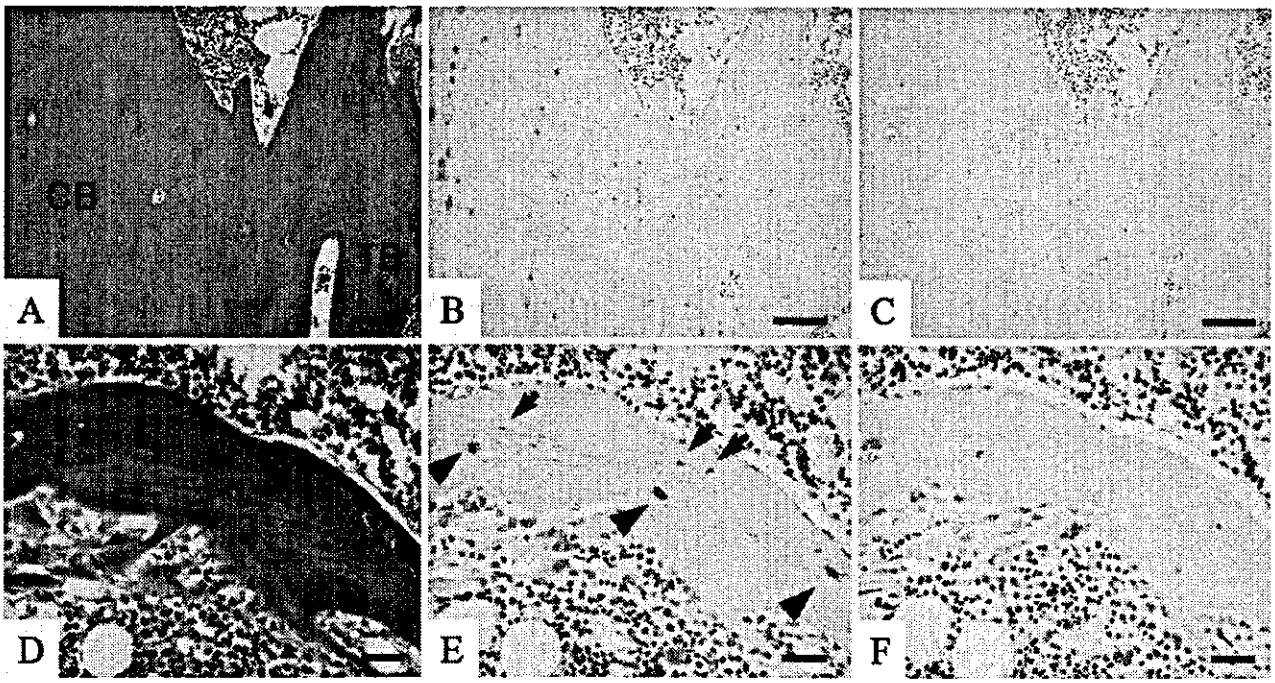

Fig. 4. Immunolocalization of MEPE in bone tissue from a patient with osteomalacia (OM1); **A,D** H&E; **B,E** anti-MEPE antibody; **C,F** negative control. **B** MEPE is expressed heterogeneously by osteocytes, and there is more positive staining in cortical bone (*CB*) than in trabecular bone (*TB*). **E** In trabecular bone, MEPE-positive cells are more abundant in the central area (*arrowheads*) than at the boundary zone (*arrows*). *Bar*, 100 μm in **A–C**; *bar*, 40 μm in **D–F**

of bone than at the boundary zone, which could be regarded as osteoid (Fig. 4E).

Abundant MEPE expression in mineralized bone in patients with osteomalacia and osteoporosis

To assess the expression of MEPE in osteoid, we performed Villanueva staining and MEPE immunostaining of bone specimens from osteomalacia patients, using serial sections. In the specimen from osteomalacia patient 1 (OM1), Villanueva staining revealed prominent osteoid at the boundaries of trabecular bone (Fig. 5A, B), and MEPE expression was mainly observed in the Villanueva-unstained mineralized bone area (Fig. 5C). In the other three osteomalacia patients, similar findings were obtained. In order to make a comparison with the pattern of MEPE localization in patients with osteoporosis, iliac bone specimens from the four osteoporosis patients were examined by the same method (Fig. 6). MEPE-positive osteocytes were mainly observed in the mineralized bone area (Fig. 6C), as was the case in the osteomalacia patients. All four osteoporosis patients showed a similar pattern of MEPE expression.

The MEPE-positive osteocyte ratio was calculated separately for mineralized bone and non-mineralized osteoid. In mineralized bone from the osteomalacia and osteoporosis patients, MEPE positivity was seen in 87.5 ± 8.6% and 95.3 ± 0.5% of the osteocytes, respectively (Table 2). In contrast, in the osteocytes in the non-mineralized osteoid of osteomalacia patients, MEPE positivity was shown in 7.8 ± 6.4%, while in the osteocytes in osteoid from osteoporosis patients MEPE positivity was shown in 4.9 ± 5.7% (Table 2). These findings show that there is significantly increased MEPE expression in the osteocytes within mineralized bone ($*P < 0.05$) in both osteomalacia and osteoporosis patients, and that there are no significant differences in MEPE expression between these two metabolic bone diseases.

Discussion

In the present study, we developed a rabbit polyclonal antibody that targeted rhMEPE expressed in *E. coli* and then used it to prepare an affinity-purified anti-MEPE antibody. Specific detection of crude rhMEPE from *E. coli* and CHO cells by Western blotting with the anti-MEPE antibody (Fig. 1) demonstrated its high specificity for MEPE. The difference in the molecular weight of MEPE obtained from *E. coli* and CHO transformants suggested that glycosylation of this molecule occurred in CHO cells.

Using this antibody, we investigated the distribution of MEPE in normal human bone by immunohistochemistry and recognized its predominant expression in bone-embedded osteocytes, a finding compatible with the results already obtained in mice [6] and rats [4]. Furthermore, MEPE expression was observed in the dendritic processes and pericellular bone matrix of the osteocytes, but not in osteoblasts.

Previous in vitro studies have suggested a correlation between MEPE expression and bone mineralization. Petersen et al. [4] showed that MEPE mRNA was expressed by fully differentiated osteoblasts and that its expression increased markedly during osteoblast-mediated mineralization of the bone matrix. Argiro et al. [5] reported a correlation between MEPE expression and bone mineralization after the addition of glycerophosphate to osteoblast culture medium. We found abundant MEPE expression by osteocytes in mineralized bone matrix, but more limited expression in non-mineralized osteoid (Figs. 5, 6), using a previously reported combination of histomorphometry and immunohistochemistry [8]. In normal bone, the non-mineralized osteoid area is too small to allow the detection of osteocytes in the non-mineralized matrix by standard histological examination. This may account for the fact that previous immunohistochemical studies of normal rodent bone did not detect osteocytes without MEPE expression. Our results, combined with previous in vitro data, suggest that MEPE is strongly expressed during the mineralization of bone as osteoblasts undergo maturation into osteocytes. However, it is not clear whether MEPE expression precedes the onset of mineralization of the bone matrix or whether it is preceded by mineralization.

Osteocytes are easily defined by their location and typical stellate morphology, and they have a relatively small number of organelles, which are necessary for the production and secretion of bone matrix [9,10]. Several non-collagenous matrix proteins have been found in and around osteoblasts and osteocytes, including OPN [11–16], osteocalcin [17–19], BSP [20–22], biglycan [23–25], osteonectin [26], and DMP1 [27–29]. These proteins are thought to play various roles in promoting bone mineralization [30] and in facilitating the attachment of osteocytes to the bone matrix [31], and genetic studies with knockout animal models have supported such hypotheses [32–36]. Some of these proteins belong to the SIBLING family, sharing many characteristic motifs and structural features (such as the RGD motif and ASARM motif encoded on chromosome 4q), and are considered to have similar functions [3]. Because most of these proteins are expressed by both osteocytes and osteoblasts, few osteocyte-specific markers have been established, apart from DMP1 [29] and several monoclonal antibodies directed against avian osteocytes (mAb OB7.3 [37], mAb OB37.11 [38], and mAb SB5 [39]). Recently, mAb OB7.3 was shown to target

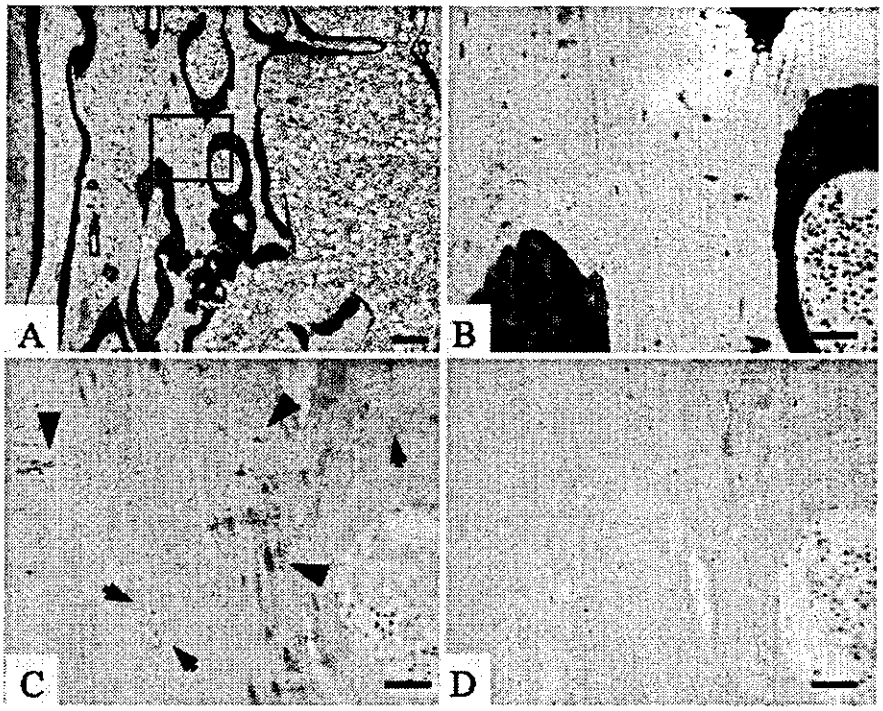

Fig. 5. Immunolocalization of MEPE in osteocytes of iliac bone tissue from a patient with oncogenic hypophosphatemic osteomalacia (OHO; OM1); **A,B** Villanueva bone stain; **C** anti-MEPE antibody; **D** negative control. **B** Higher magnification of the *boxed area in A*. **A** Abundant Villanueva-positive osteoid area is observed. **C** MEPE is expressed by osteocytes within the Villanueva-unstained mineralized bone area (*arrowheads*) and is not expressed by osteocytes within the osteoid (*arrows*). *Bar*, 150 μm in **A**; *bar*, 40 μm in **B–D**

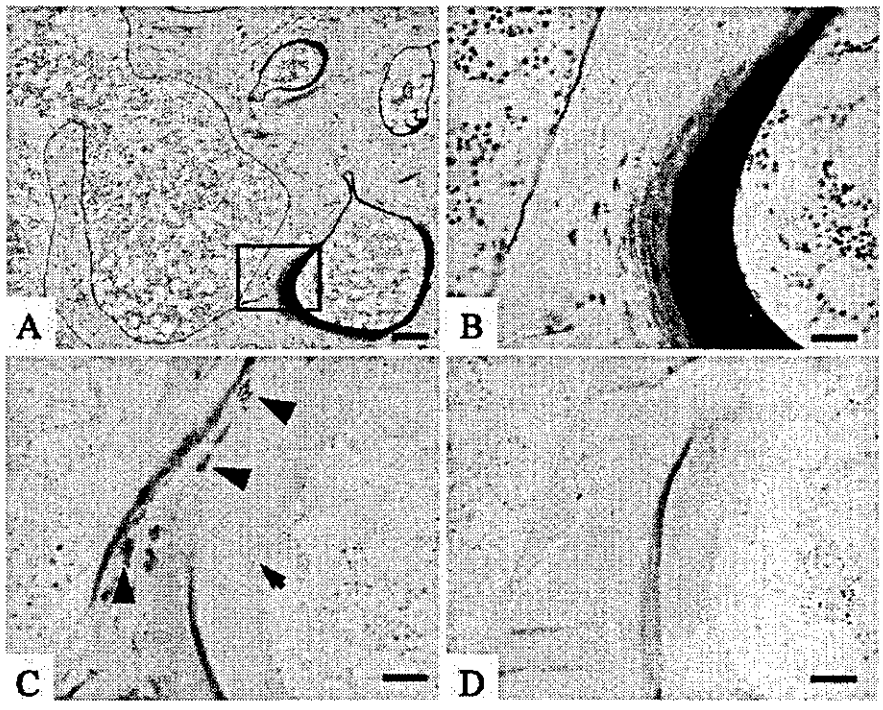

Fig. 6. Immunolocalization of MEPE in osteocytes of iliac bone tissue from a patient with osteoporosis (OP1); **A,B** Villanueva bone stain; **C** anti-MEPE antibody; **D** negative control. **B** Higher magnification of the *boxed area in A*. **A** The Villanueva-positive osteoid area is very small. **C** An osteocyte within the osteoid does not express MEPE (*arrow*), but osteocytes within mineralized bone express MEPE (*arrowheads*), as was the case in osteomalacia bone (Fig. 5). *Bar*, 150 μm in **A**; *bar*, 40 μm in **B–D**

the Phex (phosphate-regulating gene with homologies to endopeptidases on the X chromosome) protein [40]. MEPE has already been shown immunohistochemically to be expressed by rodent osteocytes, and we also demonstrated here that it is expressed predominantly in human osteocytes, but not in osteoblasts. These findings raise the possibility that MEPE is one of the specific markers for osteocytes.

We were unable to detect a difference in the distribution of MEPE between OHO and non-OHO bone

Table 2. Number of matrix extracellular phosphoglycoprotein (MEPE)-positive osteocytes and MEPE positivity in bone tissue of osteomalacia and osteoporosis patients

	Mineralized bone			Osteoid		
Patient	Total OCY	MEPE(+) OCY	Positivity (%)	Total OCY	MEPE(+) OCY	Positivity (%)
OM1	88	66	75.0	52	9	17.3
OM2	223	211	94.6	104	5	4.8
OM3	191	173	90.6	74	3	4.1
OM4	127	114	89.8	83	4	4.8
Mean ± SD value			87.5 ± 8.6			7.8 ± 6.4*
OP1	156	148	94.9	6	0	0
OP2	147	121	96.0	9	1	11.1
OP3	61	58	95.1	6	0	0
OP4	164	156	95.1	12	1	8.3
Mean ± SD value			95.3 ± 0.5			4.9 ± 5.7*

Number of osteocytes is the total value in five examined fields
OCY, number of osteocytes; MEPE(+) OCY, number of MEPE-positive osteocytes; positivity, the ratio of MEPE-positive osteocytes/total osteocytes
Asterisk indicates significant difference between positivity in mineralized bone and in osteoid, calculated by Mann-Whitney *U*-test (*$P < 0.05$)

(Table 2), or between osteoporosis and osteomalacia (Figs. 5 and 6, Table 2), so it remains unclear whether MEPE has a direct effect on bone metabolism in patients with osteomalacia. Further investigations are therefore needed to assess the influence of MEPE on bone metabolism in osteomalacia.

In summary, we demonstrated MEPE expression by osteocytes in human bone histologically, using a new rabbit polyclonal anti-rhMEPE antibody. We also investigated MEPE expression in bone from patients with osteomalacia and osteoporosis, and found that it was abundant in osteocytes within mineralized bone in both these diseases.

References

1. Rowe PS, de Zoysa PA, Dong R, Wang HR, White KE, Econs MJ, Oudet CL (2000) MEPE, a new gene expressed in bone marrow and tumors causing osteomalacia. Genomics 67:54–68
2. De Beur SM, Finnegan RB, Vassiliadis J, Cook B, Barberio D, Estes S, Manavalan P, Petroziello J, Madden SL, Cho JY, Kumar R, Levine MA, Schiavi SC (2002) Tumors associated with oncogenic osteomalacia express genes important in bone and mineral metabolism. J Bone Miner Res 17:1102–1110
3. Fisher LW, Torchia DA, Fohr B, Young MF, Fedarko NS (2001) Flexible structures of SIBLING proteins, bone sialoprotein, and osteopontin. Biochem Biophys Res Commun 280:460–465
4. Petersen DN, Tkalcevic GT, Mansolf AL, Rivera-Gonzalez R, Brown TA (2000) Identification of osteoblast/osteocyte factor 45 (OF45), a bone-specific cDNA encoding an RGD-containing protein that is highly expressed in osteoblasts and osteocytes. J Biol Chem 275:36172–36180
5. Argiro L, Desbarats M, Glorieux FH, Ecarot B (2001) Mepe, the gene encoding a tumor-secreted protein in oncogenic hypophosphatemic osteomalacia, is expressed in bone. Genomics 74:342–351
6. Gowen LC, Petersen DN, Mansolf AL, Qi H, Stock JL, Tkalcevic GT, Simmons HA, Crawford DT, Chidsey-Frink KL, Ke HZ, McNeish JD, Brown TA (2003) Targeted disruption of the osteoblast/osteocyte factor 45 gene (OF45) results in increased bone formation and bone mass. J Biol Chem 278:1998–2007
7. Kawai Y, Morimoto S, Sakaguchi K, Yoshino H, Yotsui T, Hirota S, Inohara H, Nakagawa T, Hattori K, Kubo T, Yang J, Fujiwara N, Ogihara T (2001) Oncogenic osteomalacia secondary to nasal tumor with decreased urinary excretion of cAMP. J Bone Miner Metab 19:61–64
8. Derkx P, Nigg AL, Bosman FT, Birkenhager-Frenkel DH, Houtsmuller AB, Pols HA, van Leeuwen JP (1998) Immunolocalization and quantification of noncollagenous bone matrix proteins in methylmethacrylate-embedded adult human bone in combination with histomorphometry. Bone 22:367–373
9. Aarden EM, Burger EH, Nijweide PJ (1994) Function of osteocytes in bone. J Cell Biochem 55:287–299
10. Nijweide PJ, Burger EH, Klein-Nulend J (2002) The osteocyte. In: Bilezikian J, Raisz L, Rodan G (eds) Principles of Bone Biology, 2nd edn. Academic, San Diego, pp 93–107
11. Fisher LW, Hawkins GR, Tuross N, Termine JD (1987) Purification and partial characterization of small proteoglycans I and II, bone sialoproteins I and II, and osteonectin from the mineral compartment of developing human bone. J Biol Chem 262:9702–9708
12. Franzen A, Heinegard D (1985) Isolation and characterization of two sialoproteins present only in bone calcified matrix. Biochem J 232:715–724
13. Mark MP, Butler WT, Prince CW, Finkelman RD, Ruch JV (1988) Developmental expression of 44-kDa bone phosphoprotein (osteopontin) and bone gamma-carboxyglutamic acid (Gla)-containing protein (osteocalcin) in calcifying tissues of rat. Differentiation 37:123–136
14. Mark MP, Prince CW, Oosawa T, Gay S, Bronckers AL, Butler WT (1987) Immunohistochemical demonstration of a 44-KD phosphoprotein in developing rat bones. J Histochem Cytochem 35:707–715
15. Prince CW, Oosawa T, Butler WT, Tomana M, Bhown AS, Bhown M, Schrohenloher RE (1987) Isolation, characterization, and biosynthesis of a phosphorylated glycoprotein from rat bone. J Biol Chem 262:2900–2907
16. Young MF, Kerr JM, Termine JD, Wewer UM, Wang MG, McBride OW, Fisher LW (1990) cDNA cloning, mRNA distribution and heterogeneity, chromosomal location, and RFLP analysis of human osteopontin (OPN). Genomics 7:491–502

17. Boivin G, Morel G, Lian JB, Anthoine-Terrier C, Dubois PM, Meunier PJ (1990) Localization of endogenous osteocalcin in neonatal rat bone and its absence in articular cartilage: effect of warfarin treatment. Virchows Arch A Pathol Anat Histopathol 417:505–512
18. Hauschka PV, Lian JB, Gallop PM (1975) Direct identification of the calcium-binding amino acid, gamma-carboxyglutamate, in mineralized tissue. Proc Natl Acad Sci USA 72:3925–3929
19. Ohta T, Mori M, Ogawa K, Matsuyama T, Ishii S (1989) Immunocytochemical localization of BGP in human bones in various developmental stages and pathological conditions. Virchows Arch A Pathol Anat Histopathol 415:459–466
20. Chen J, Zhang Q, McCulloch CA, Sodek J (1991) Immunohistochemical localization of bone sialoprotein in foetal porcine bone tissues: comparisons with secreted phosphoprotein 1 (SPP-1, osteopontin) and SPARC (osteonectin). Histochem J 23:281–289
21. Chen JK, Shapiro HS, Wrana JL, Reimers S, Heersche JN, Sodek J (1991) Localization of bone sialoprotein (BSP) expression to sites of mineralized tissue formation in fetal rat tissues by in situ hybridization. Matrix 11:133–143
22. Oldberg A, Franzen A, Heinegard D (1988) The primary structure of a cell-binding bone sialoprotein. J Biol Chem 263:19430–19432
23. Bianco P, Fisher LW, Young MF, Termine JD, Robey PG (1990) Expression and localization of the two small proteoglycans biglycan and decorin in developing human skeletal and non-skeletal tissues. J Histochem Cytochem 38:1549–1563
24. Ibaraki K, Termine JD, Whitson SW, Young MF (1992) Bone matrix mRNA expression in differentiating fetal bovine osteoblasts. J Bone Miner Res 7:743–754
25. Ingram RT, Clarke BL, Fisher LW, Fitzpatrick LA (1993) Distribution of noncollagenous proteins in the matrix of adult human bone: evidence of anatomic and functional heterogeneity. J Bone Miner Res 8:1019–1029
26. Jundt G, Berghauser KH, Termine JD, Schulz A (1987) Osteonectin—a differentiation marker of bone cells. Cell Tissue Res 248:409–415
27. D'Souza RN, Cavender A, Sunavala G, Alvarez J, Ohshima T, Kulkarni AB, MacDougall M (1997) Gene expression patterns of murine dentin matrix protein 1 (Dmp1) and dentin sialophosphoprotein (DSPP) suggest distinct developmental functions in vivo. J Bone Miner Res 12:2040–2049
28. MacDougall M, Gu TT, Luan X, Simmons D, Chen J (1998) Identification of a novel isoform of mouse dentin matrix protein 1: spatial expression in mineralized tissues. J Bone Miner Res 13:422–431
29. Toyosawa S, Shintani S, Fujiwara T, Ooshima T, Sato A, Ijuhin N, Komori T (2001) Dentin matrix protein 1 is predominantly expressed in chicken and rat osteocytes but not in osteoblasts. J Bone Miner Res 16:2017–2026
30. Robey PG (1996) Vertebrate mineralized matrix proteins: structure and function. Connect Tissue Res 35:131–136
31. Aarden EM, Nijweide PJ, van der Plas A, Alblas MJ, Mackie EJ, Horton MA, Helfrich MH (1996) Adhesive properties of isolated chick osteocytes in vitro. Bone 18:305–313
32. Delany AM, Amling M, Priemel M, Howe C, Baron R, Canalis E (2000) Osteopenia and decreased bone formation in osteonectin-deficient mice. J Clin Invest 105:915–923
33. Ducy P, Desbois C, Boyce B, Pinero G, Story B, Dunstan C, Smith E, Bonadio J, Goldstein S, Gundberg C, Bradley A, Karsenty G (1996) Increased bone formation in osteocalcin-deficient mice. Nature 382:448–452
34. Rittling SR, Matsumoto HN, McKee MD, Nanci A, An XR, Novick KE, Kowalski AJ, Noda M, Denhardt DT (1998) Mice lacking osteopontin show normal development and bone structure but display altered osteoclast formation in vitro. J Bone Miner Res 13:1101–1111
35. Xu T, Bianco P, Fisher LW, Longenecker G, Smith E, Goldstein S, Bonadio J, Boskey A, Heegaard AM, Sommer B, Satomura K, Dominguez P, Zhao C, Kulkarni AB, Robey PG, Young MF (1998) Targeted disruption of the biglycan gene leads to an osteoporosis-like phenotype in mice. Nat Genet 20:78–82
36. Yoshitake H, Rittling SR, Denhardt DT, Noda M (1999) Osteopontin-deficient mice are resistant to ovariectomy-induced bone resorption. Proc Natl Acad Sci USA 96:8156–8160
37. Nijweide PJ, Mulder RJ (1986) Identification of osteocytes in osteoblast-like cell cultures using a monoclonal antibody specifically directed against osteocytes. Histochemistry 84:342–347
38. Nijweide PJ, van der Plas A, Olthof AA (1988) Osteoblastic differentiation. Ciba Found Symp 136:61–77
39. Bruder SP, Caplan AI (1990) Terminal differentiation of osteogenic cells in the embryonic chick tibia is revealed by a monoclonal antibody against osteocytes. Bone 11:189–198
40. Westbroek I, De Rooij KE, Nijweide PJ (2002) Osteocyte-specific monoclonal antibody MAb OB7.3 is directed against Phex protein. J Bone Miner Res 17:845–853

JCB Article

Smad6/Smurf1 overexpression in cartilage delays chondrocyte hypertrophy and causes dwarfism with osteopenia

Mitsuru Horiki,[1] Takeshi Imamura,[2] Mina Okamoto,[1] Makoto Hayashi,[2] Junko Murai,[1] Akira Myoui,[1] Takahiro Ochi,[1] Kohei Miyazono,[2,3] Hideki Yoshikawa,[1] and Noriyuki Tsumaki[1]

[1]Department of Orthopaedics, Osaka University Graduate School of Medicine, Osaka 565-0871, Japan
[2]Department of Biochemistry, The Cancer Institute of the Japanese Foundation for Cancer Research, Tokyo 170-8455, Japan
[3]Department of Molecular Pathology, Graduate School of Medicine, University of Tokyo, Tokyo 113-0033, Japan

Biochemical experiments have shown that Smad6 and Smad ubiquitin regulatory factor 1 (Smurf1) block the signal transduction of bone morphogenetic proteins (BMPs). However, their in vivo functions are largely unknown. Here, we generated transgenic mice overexpressing Smad6 in chondrocytes. Smad6 transgenic mice showed postnatal dwarfism with osteopenia and inhibition of Smad1/5/8 phosphorylation in chondrocytes. Endochondral ossification during development in these mice was associated with almost normal chondrocyte proliferation, significantly delayed chondrocyte hypertrophy, and thin trabecular bone. The reduced population of hypertrophic chondrocytes after birth seemed to be related to impaired bone growth and formation. Organ culture of cartilage rudiments showed that chondrocyte hypertrophy induced by BMP2 was inhibited in cartilage prepared from Smad6 transgenic mice. We then generated transgenic mice overexpressing Smurf1 in chondrocytes. Abnormalities were undetectable in Smurf1 transgenic mice. Mating Smad6 and Smurf1 transgenic mice produced double-transgenic pups with more delayed endochondral ossification than Smad6 transgenic mice. These results provided evidence that Smurf1 supports Smad6 function in vivo.

Introduction

Bone morphogenetic proteins (BMPs) were originally identified as secreted signaling molecules that could induce ectopic endochondral bone formation when implanted subcutaneously. Subsequent molecular cloning experiments have revealed that the BMP family consists of various molecules including the growth and differentiation factor subfamily, and belongs to the TGF-β superfamily. BMP family members have diverse biological activities during the development of various organs and tissues, as well as during embryonic axis determination (Hogan, 1996).

Members of the TGF-β superfamily transduce their signals through two types of serine/threonine kinase receptors, types I and II (Heldin et al., 1997; Shi and Massague, 2003). Upon ligand binding, type I and type II receptors form a tetramer consisting of two pairs of type I and type II receptors. Type II receptors phosphorylate type I receptors. Then, type I receptors phosphorylate downstream targets such as Smads. In vertebrates, seven type I receptors and five type II receptors have been found so far. Among them, three type I receptors, BMP type IA receptor (BMPR-IA, or activin receptor-like kinase [ALK-3]), BMPR-IB (ALK-6), and ALK-2, mediate BMP signaling. Smads are the major downstream targets of type I receptors for TGF-β/BMP superfamily proteins (Heldin et al., 1997). Eight Smads have been identified in mammals and are classified into three subgroups. Receptor-regulated Smads (R-Smads) are phosphorylated at SSXS motifs at their COOH terminus by type I receptors. Smad1, Smad5, and Smad8 are R-Smads that transduce BMP signals, and Smad2 and Smad3 are responsible for TGF-β and activin signaling. Phosphorylated R-Smads form heteromers with

Address correspondence to Noriyuki Tsumaki, Dept. of Orthopaedics, Osaka University Graduate School of Medicine, 2-2 Yamadaoka, Suita, Osaka 565-0871, Japan. Tel.: 81-6-6879-3552. Fax: 81-6-6879-3559. email: tsumaki-n@umin.ac.jp

Key words: chondrocyte; hypertrophy; osteopenia; dwarfism; transgenic mice

Abbreviations used in this paper: BMP, bone morphogenetic protein; BMPR, BMP receptor; *Col10a1*, type X collagen gene; *Col11a2*, α2(XI) collagen chain gene; *Col2a1*, type II collagen gene; d.p.c., days post coitus; G_0, generation zero; rhBMP2, recombinant human BMP2; R-Smads, receptor-regulated Smads; Smurf1, Smad ubiquitin regulatory factor 1; TRAP, tartate-resistant acid phosphatase.

The Journal of Cell Biology, Volume 165, Number 3, May 10, 2004 433–445
http://www.jcb.org/cgi/doi/10.1083/jcb.200311015

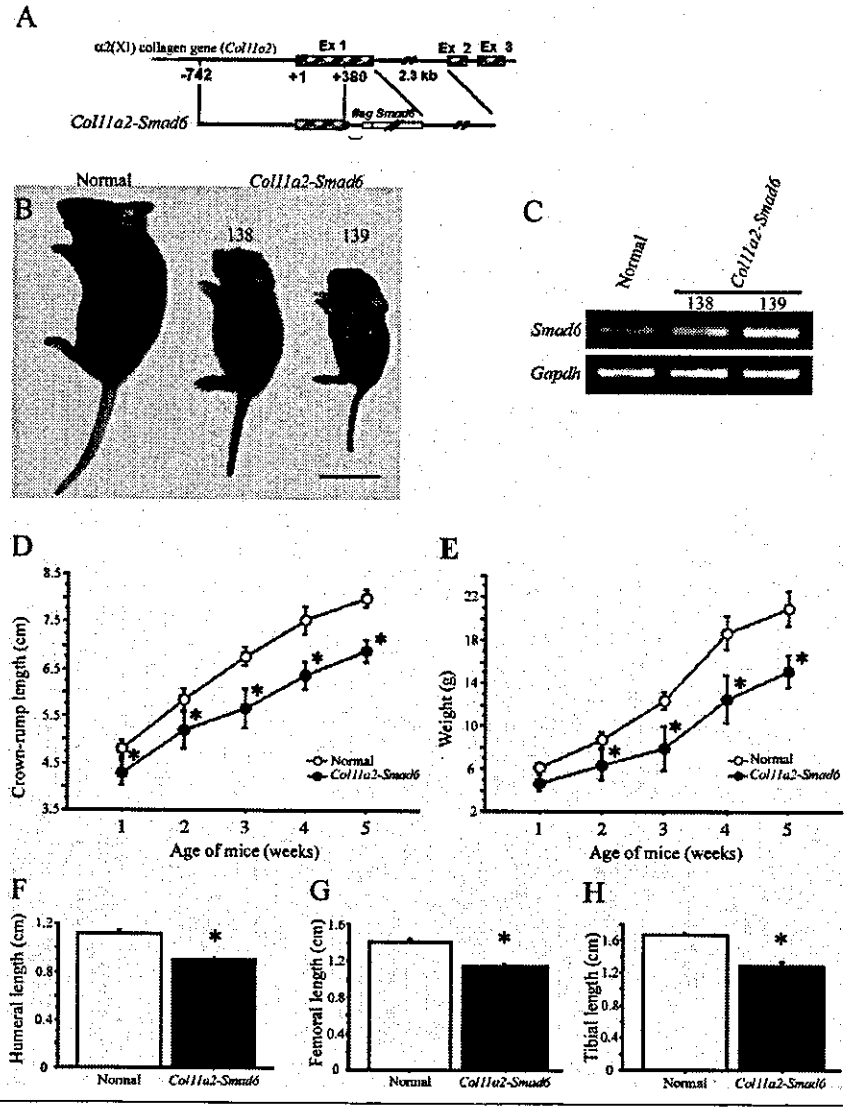

Figure 1. **Postnatal dwarfism in Smad6 transgenic mice.** (A) Diagram of DNA constructs used to generate Smad6 transgenic mice. Gene structure of *Col11a2* is shown at top. Boxes indicate coding regions and solid lines denote noncoding sequences. A 1.6-kb DNA fragment covering the entire coding region of mouse Smad6 cDNA tagged with FLAG sequence at the 5′ terminus was ligated to the promoter and 1st intron enhancer sequences of the *Col11a2* gene. Bracket indicates SV40 splice cassette. (B) Normal and transgenic pups from lines 138 and 139 at 3 wk of age. (C) RT-PCR analysis of Smad6 mRNA expression at 16.5 d.p.c. (D and E) Temporal changes in crown–rump length (D) and weight (E) of wild-type and Smad6 transgenic mice from line 199 ($n = 12$). (F–H) Length of humerus (F), femur (G), and tibia (H) in wild-type and Smad6 transgenic mice from line 199 at 3 wk of age ($n = 5$). Error bars show means ± SD. *, $P < 0.01$ between wild-type and transgenic mice as determined by *t* test. Bar (B), 3 cm.

the common-partner Smad (Smad4), and translocate into the nucleus where they interact with transcriptional factors to bind directly or indirectly to specific DNA sequences for the activation of gene transcription.

BMP signaling is subject to delicate regulation at multiple levels: extracellularly, at the membrane site, and intracellularly (Balemans and Van Hul, 2002). In the extracellular space, several molecules antagonize BMPs. Among these antagonists, noggin is expressed in cartilage and binds to BMPs and prevents them from interacting with their receptors. At the intracellular level, inhibitory Smads, Smad6 and Smad7, inhibit phosphorylation of R-Smads by competing with R-Smads for binding to phosphorylated type I receptors. In particular, Smad6 appears to inhibit BMP signaling, whereas Smad7 associates stably with TGF-β receptor and BMP receptor complexes and inhibits the TGF-β– or BMP-mediated phosphorylation of R-Smads (Hanyu et al., 2001). In addition, ubiquitin-dependent protein degradation plays key roles in Smad signaling. Smad ubiquitin regulatory factor 1 (Smurf1) and Smurf2 induce the ubiquitination and degradation of Smad1 and Smad5 (Zhu et al., 1999; Zhang et al., 2001). Furthermore, Smurf1 and Smurf2 interact with nuclear Smad7 and induce the nuclear export of Smad7. Smurf–Smad7 complexes then associate with type I receptor for TGF-β and enhance its turnover (Kavsak et al., 2000; Ebisawa et al., 2001). Recent biochemical analyses have shown that Smurf1 binds to BMP type I receptors via Smad6 and Smad7, and that it induces the ubiquitination and degradation of these receptors (Murakami et al., 2003). Thus, Smad6 and Smurf1 cooperatively down-regulate BMP signals by degradation of R-Smads as well as BMP receptors. However, the physiological function of Smurfs is unknown.

During development, the limb skeleton is formed through endochondral bone formation (Erlebacher et al., 1995). Mesenchymal cells initially undergo condensation followed by differentiation of cells within these condensations into chondrocytes. Chondrocytes then proliferate and produce ECM to form primordial cartilage. Shortly after the primordial cartilage formation, proliferating chondrocytes in the central region of the cartilage undergo terminal differentia-

tion to hypertrophic chondrocytes. Hypertrophic chondrocytes exit the cell cycle and synthesize an ECM that is different in composition from that of proliferating cartilage. The hypertrophic cartilage is invaded by blood vessels along with osteoblasts, osteoclasts, and hematopoietic cells to form primary ossification centers. Within these centers, the hypertrophic cartilage matrix is degraded, hypertrophic chondrocytes die, and osteoblasts replace the disappearing cartilage with trabecular bone (Olsen et al., 2000). Then, bone formation and maintenance are performed by a balance between the new apposition of bony matrix by osteoblasts and resorption by osteoclasts.

Smad proteins have been identified in growth plate cartilage (Flanders et al., 2001). In vitro analyses have shown that Smad6 regulates the chondrocytic phenotype (Valcourt et al., 2002; Nishihara et al., 2003). However, the physiological roles of Smad6 and Smad signaling in normal endochondral bone formation have not been determined. Here, we generated transgenic mice overexpressing Smad6 or Smurf1 in chondrocytes under the control of the α2(XI) collagen chain gene (*Col11a2*) promoter/enhancer sequences. We found that overexpression of Smad6 does not significantly affect chondrocyte proliferation, but significantly delays chondrocyte hypertrophy, which may lead to postnatal dwarfism with osteopenia. By using double-transgenic mice, we also found that Smurf1 supports Smad6 function in vivo.

Results

Generation of Smad6 transgenic mouse lines

We ligated the Smad6 cDNA with a 5′ FLAG epitope to *Col11a2* promoter/enhancer sequences to construct the transgene *Col11a2-Smad6* (Fig. 1 A). Generation zero (G_0) embryos of Smad6 transgenic mice were initially killed, in case Smad6 transgenic mice were lethal. 17 of 129 embryos were genetically positive for the transgene. Smad6 transgenic and normal embryos appeared similar. The Smad6 transgenic mice survived after birth, so several independent transgenic mouse lines could be established. The phenotypes of all transgenic mouse lines were similar, with differences in the degree of abnormalities between lines.

Postnatal dwarfism in Smad6 transgenic mice

1 wk after birth, the Smad6 transgenic mice started to develop dwarfism (Fig. 1, B–H). Our data were collected from three transgenic founders derived from microinjections, transgenic pups with severe phenotypes generated from two mosaic founders (lines 138 and 139), and transgenic offspring with mild phenotypes generated from two transgenic founders (lines 165 and 199). Dwarfism was more severe in the transgenic mice of line 139 than of line 138 (Fig. 1 B). Phenotype severity closely correlated with transgene expression levels as shown by RT-PCR (Fig. 1 C). Quantitative real-time RT-PCR using total RNAs extracted from limb buds showed that the amount of Smad6 mRNAs of transgenic line 139 was threefold that of normal mice, and double that of transgenic line 138. At 3 wk after birth, the average crown–rump length of transgenic mice (line 199) was ~20% shorter than that of normal mice (Fig. 1 D). Transgenic mice (line 199) weighed an average of 30–40% less (Fig. 1 E), and

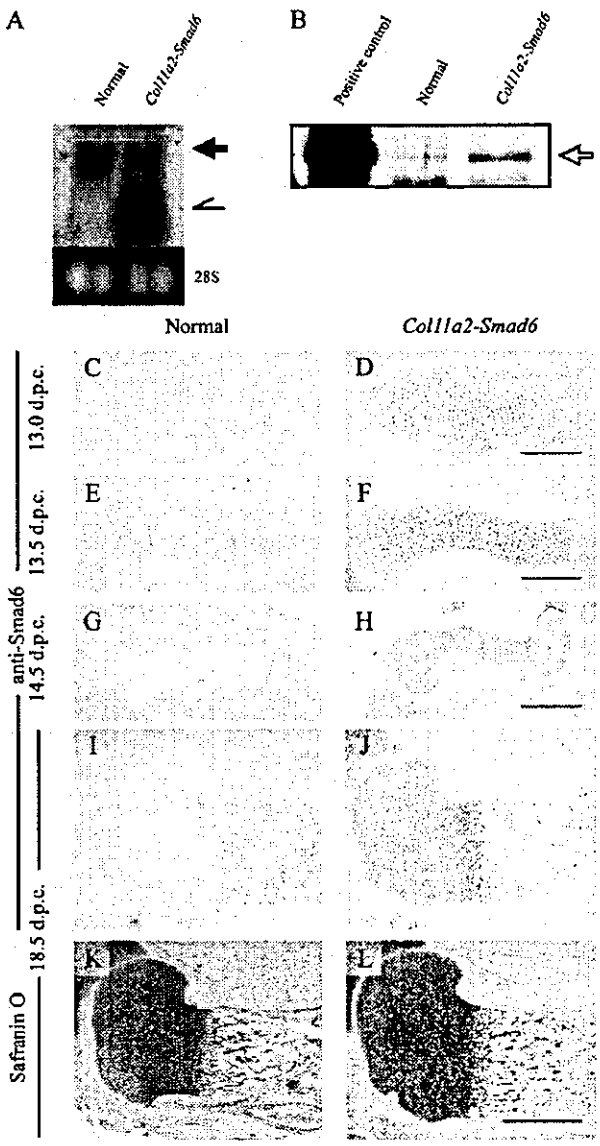

Figure 2. **Cartilage-specific expression of transgene in Smad6 transgenic mice.** (A) Northern blot hybridized with Smad6 probe. Bottom shows ethidium bromide–stained gel before transfer. (B) Protein expression of Smad6 transgene. Positive control consisted of lysates from COS7 cells transfected with expression construct FLAG-Smad6 (left lane). (C–L) Immunohistochemical analysis of humerus from normal (C, E, G, and I) and Smad6 (D, F, H, and J) transgenic mice at various stages of development using anti-Smad6 antibody. Serial sections for I and J were stained with safranin O/fast green/iron hematoxylin (K and L). Arrow indicates endogenous Smad6 mRNA. Half-arrow indicates Smad6 transgene mRNA. Open arrow represents FLAG-tagged Smad6 protein. Bars: (C and D) 100 μm; (E and F) 200 μm; (G–L) 500 μm.

the average length of the skeletal components was 20–30% shorter compared with normal littermates (Fig. 1, F–H).

Cartilage-specific expression of transgene in Smad6 transgenic mice

Northern blotting demonstrated Smad6 expression in the limb buds of transgenic mice. Transgene Smad6 mRNA was

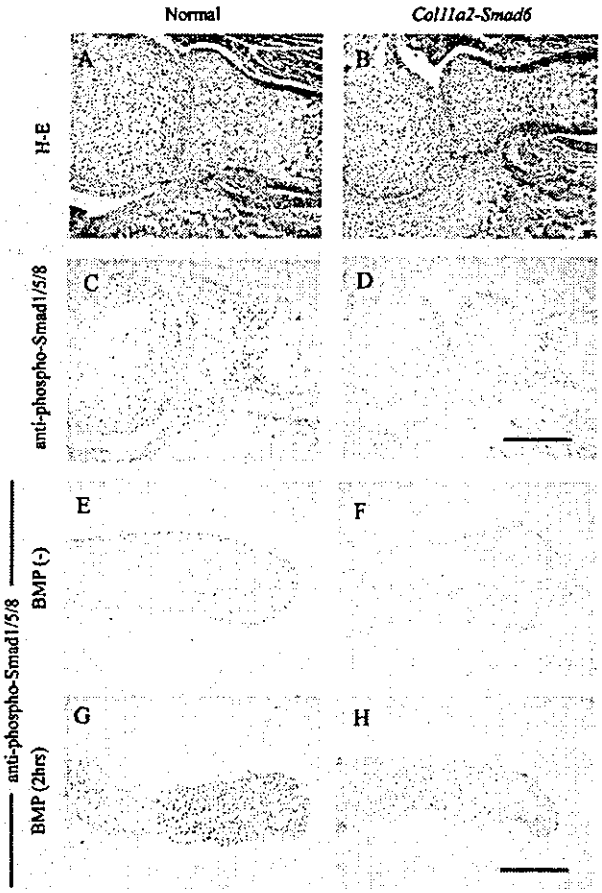

Figure 3. **Blockage of Smad signaling in cartilage of Smad6 transgenic mice.** (A–D) Immunohistochemistry of elbow joints in wild-type (A and C) and transgenic (B and D) mice at 16.5 d.p.c. Staining with hematoxylin and eosin (A and B). Serial sections of A and B were immunostained using anti-phospho-Smad1/5/8 antibody (C and D). (E–H) Immunohistochemistry of metatarsal cartilage explants at 15.0 d.p.c. before (E and F) and after exposure to rhBMP2 for 2 h (G and H). Phospho-Smad1/5/8 immunoreactivity was not increased by rhBMP2 in sections of cartilage explants from Smad6 transgenic mice (F and H) compared with those in wild-type mice (E and G). Bars: (A–D) 300 μm; (E–H) 200 μm.

~2 kb in length, which was smaller than endogenous Smad6 mRNA due to shorter 5′ and 3′ untranslated regions (Fig. 2 A). Immunoblotting demonstrated the expression of a 70-kD FLAG-tagged Smad6 protein in limb buds of Smad6 transgenic mice (Fig. 2 B, open arrow). Immunohistochemistry using anti-Smad6 antibody showed more intense signals for Smad6 proteins in forelimb chondrocytes of Smad6 transgenic mice (Fig. 2, D, F, H, and J) than from wild-type mice (Fig. 2, C, E, G, and I) from 13.0 through 18.5 days post coitus (d.p.c.).

Blockage of Smad signaling in cartilage of Smad6 transgenic mice

We examined Smad signaling in chondrocytes by immunohistochemistry using an antibody that recognizes only phosphorylated forms of Smad1, Smad5, and Smad8. Phospho-Smad1/5/8 immunoreactivity was reduced in transgenic cartilage sections from 16.5 d.p.c. limbs (Fig. 3, B and D) compared with the wild type (Fig. 3, A and C). We cultured explants of metatarsal primordial cartilage from 15.0 d.p.c. embryos. Recombinant human BMP2 (rhBMP2) proteins were added to the culture media and explants were histologically analyzed 2 h later. rhBMP2 dramatically increased phospho-Smad1/5/8 immunoreactivity in explants from wild-type mice (Fig. 3, E and G), but not from Smad6 transgenic mice (Fig. 3, F and H). These results suggested that Smad signaling was inhibited in the transgenic cartilage by an excess of Smad6.

Osteopenia in Smad6 transgenic mice

We analyzed the bone structure of transgenic mice. Micro-CT analysis of the humerus revealed that the primary spongiosa was significantly more hypoplastic and disorganized in Smad6 transgenic mice (Fig. 4, B and D) than in normal littermates (Fig. 4, A and C). The average bone volume per total tissue volume of primary spongiosa was 30–40% smaller than that of normal littermates (Fig. 4 E).

Differences in bone formation were further examined by bone histomorphometric analysis. Trabecular bone volume was significantly decreased in Smad6 transgenic mice (Fig. 4 F). The osteoblast surface per bone surface in transgenic mice was significantly decreased (Fig. 4 G). We analyzed dynamic changes in bone formation and mineralization by injecting tetracycline and calcein at 2-d intervals. The distance between the two consecutive labels was significantly decreased in transgenic mice (Fig. 4, H–J). The mineralization surface was decreased, although not significantly (Fig. 4 K). These data showed a significantly decreased bone formation rate (Fig. 4 L). As for osteoclastic bone resorption, the osteoclast number per bone surface, osteoclast surface per bone surface, and erosive surface per bone surface were significantly increased (Fig. 4, M–O).

To elucidate the mechanism by which osteoclastic bone resorption was activated in Smad6 transgenic mice, we performed bone marrow cell culture and analyzed dexamethasone/parathyroid hormone-induced osteoclastogenesis. The number of tartrate-resistant acid phosphatase (TRAP)–positive multinucleated cells in the culture prepared from transgenic mice was equivalent to that of normal mice (Fig. 4, P–R). The resorption of hydroxyapatite by cultured osteoclast prepared from transgenic mice was essentially normal (Fig. 4 S). Next, we examined osteoclast formation activities in spleen cell culture in the presence of RANK ligand. RANK ligand–induced osteoclastogenesis of spleen cells from Smad6 transgenic mice was normal, as indicated by the number of TRAP-positive multinucleated cells and the resorption of hydroxyapatite (unpublished data). These results suggested that both osteoclast precursors and osteoclast-supporting activities of osteoblast/stromal cells were normal in the bone marrow of Smad6 transgenic mice.

Skeletal development of Smad6 transgenic mice

Because the transgene was expressed specifically in cartilage, we analyzed the skeleton from earlier stages of development. Whole-mount in situ hybridization using a type II collagen gene (*Col2a1*) antisense cRNA probe showed that the pattern and intensity of signals did not obviously differ between

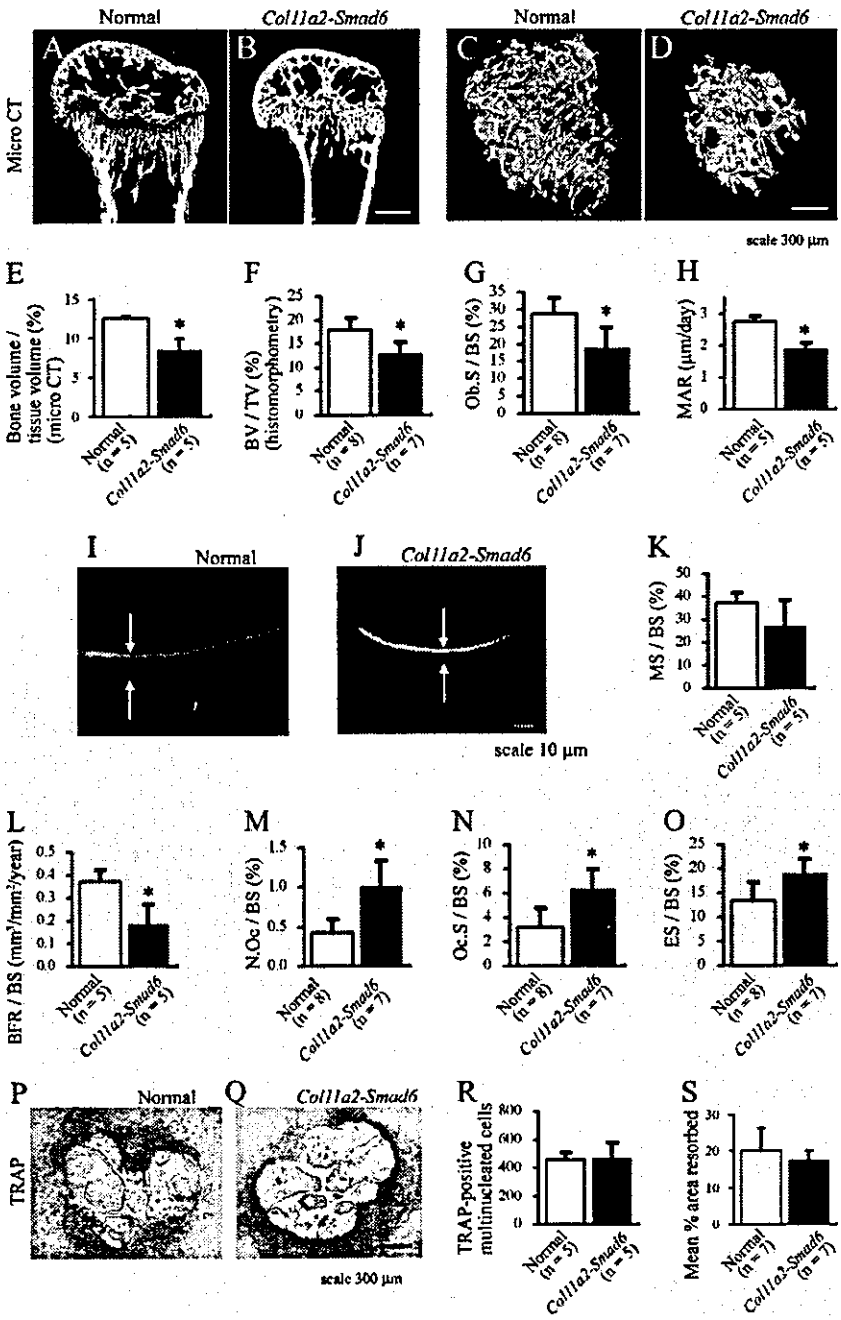

Figure 4. **Osteopenia in Smad6 transgenic mice.** (A–E) Micro-CT analysis of proximal humerus in 3-wk-old normal (A and C) and Smad6 transgenic (B and D) mice. Reconstructed coronal view (A and B) and reconstructed three-dimensional image (C and D) of trabecular bone. (E) Trabecular bone volume per total tissue volume compared between normal and transgenic mice. (F–O) Bone histomorphometric analysis of fourth lumbar vertebral bodies at 4 wk of age. (F) Trabecular bone volume (BV/TV; bone volume over tissue volume), (G) osteoblast surface per bone surface (Ob.S/BS), (H) mineral apposition rate (MAR), (K) mineralizing surface per bone surface (MS/BS), (L) bone-forming rate per bone surface (BFR/BS), (M) osteoclast number per bone surface (N.Oc/BS), (N) osteoclast surface per bone surface (Oc.S/BS), and (O) eroded surface per bone surface (ES/BS) compared between normal and transgenic mice. Fluorescent micrograph of labeled mineralization fronts in normal (I) and Smad6 transgenic (J) mice. (P–S) Osteoclastogenesis of cultured bone marrow cells. Micrograph of cultured multinucleated cells stained with TRAP prepared from normal (P) and Smad6 transgenic (Q) mice. Number of TRAP-positive multinucleated cells (R) and resorption of hydroxyapatite (S) were compared between normal and transgenic mice. Error bars show means ± SD. *, $P < 0.01$ between normal and transgenic mice as determined by *t* test. Bars: (A–D, P, and Q) 300 μm; (I and J) 10 μm.

Smad6 transgenic and normal mice at either 12.5 (Fig. 5, A and B) or 13.0 (Fig. 5, C and D) d.p.c. This suggested that mesenchymal condensation was essentially normal in the transgenic mice. At 13.5 d.p.c., the size and shape of each cartilaginous skeletal component stained with Alcian blue of transgenic mice were essentially identical to those of normal littermates (Fig. 5, E and F). The central regions of metatarsals were mineralized in normal mice as they were stained with Alizarin red S, but not in transgenic mice at 16.5 d.p.c. (Fig. 5, G and H, arrowheads) and at 18.5 d.p.c. (Fig. 5, I and J, arrowheads). The size of mineralized tissue in the humerus and femur was considerably smaller in transgenic mice than in normal mice (Fig. 5, G and H, arrows). At 3 wk of age, skeleton of transgenic mice was much smaller than that of normal mice (Fig. 5, K and L).

Delayed hypertrophy of chondrocytes in Smad6 transgenic mice

We further examined endochondral bone formation by histological means. At 13.5 d.p.c. when condensed mesenchymal cells differentiate into chondrocytes, chondrocytes did not obviously differ histologically between normal and transgenic mice (Fig. 6, A and B). At 14.5 d.p.c., proliferative chondrocytes exit the cell cycle and start terminal differ-

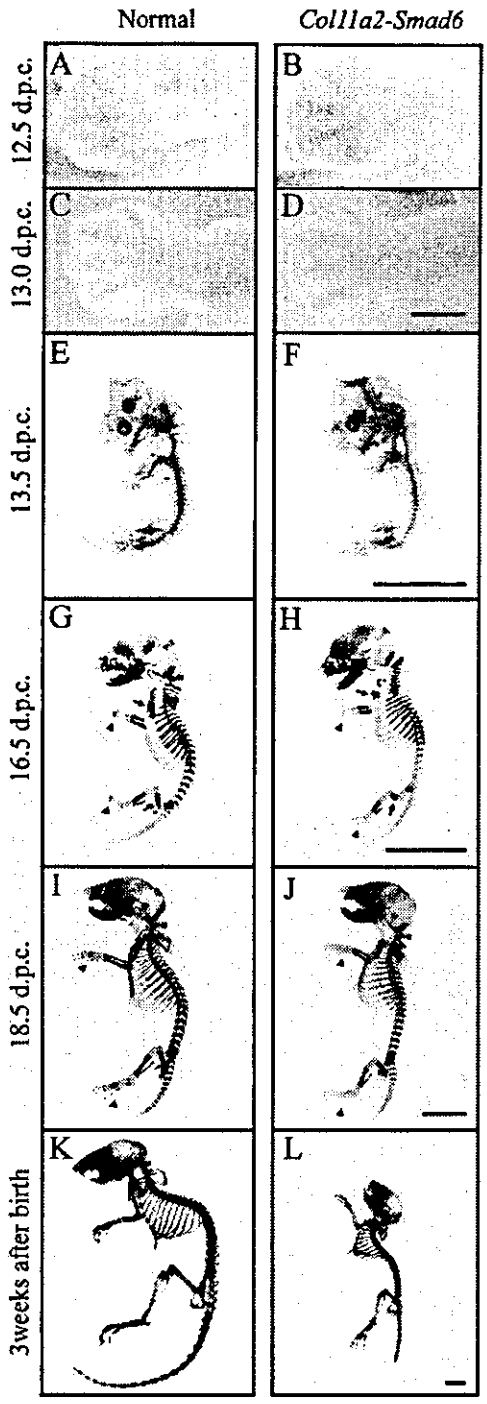

Figure 5. **Skeletal development of Smad6 transgenic mice.** (A–D) Whole-mount in situ hybridization using *Col2a1* antisense cRNA probe at 12.5 (A and B) and 13.0 (C and D) d.p.c. (E–L) Alcian blue and Alizarin red S staining of whole skeleton of normal (E, G, I, and K) and transgenic (F, H, J, and L) mice at various stages of development. Arrowheads indicate metatarsals. Arrows show mineralized tissues in humerus and femur. Bars: (A–D) 200 μm; (E–L) 2 mm.

entiation into hypertrophic chondrocytes at the center of each skeletal component (Fig. 6 C). On the other hand, transgenic cartilage from the humerus contained proliferative but not hypertrophic chondrocytes (Fig. 6 D). Hybridization in situ showed that proliferative chondrocytes in Smad6 transgenic mice expressed *Col2a1* mRNA (Fig. 6 F), like those of normal mice. Northern blotting of limb bud extracts showed that expression levels of the Sox9 gene, *Col2a1*, and type IX collagen α1 chain mRNAs were similar between transgenic and normal mice at 13.5–19.5 d.p.c. (unpublished data). However, the transgenic cartilage lacked type X collagen–positive (Fig. 6 H) and osteopontin-positive (Fig. 6 J) cells, whereas cartilage from normal mice expressed these genes (Fig. 6, G and I). In addition, von Kossa staining revealed mineralization in the normal (Fig. 6 K) but not in the transgenic (Fig. 6 L) mouse humerus. At 16.5 d.p.c., normal mice formed ossification centers in the humerus (Fig. 6 M). However, although a zone of hypertrophic chondrocytes was present in the transgenic humerus, an ossification center had not formed (Fig. 6 N). At 18.5 d.p.c., the transgenic skeletal element was composed of cartilage at both ends and bone at the center, like the wild type (Fig. 6, O and P). These results suggest that Smad6 overexpression delayed chondrocyte hypertrophy and ossification by ~3 d during development of the mouse humerus.

Normal chondrocyte proliferation and reduced population of hypertrophic chondrocytes in Smad6 transgenic mice

For further analysis of chondrocyte proliferation in Smad6 transgenic mice, we performed BrdU labeling at embryonic (Fig. 7, A and B) and postnatal (Fig. 7, C–F) stages. There were not significant differences in BrdU labeling indexes between chondrocytes of normal and Smad6 transgenic mice at 16.5 d.p.c. (Fig. 7 G) and at 3 wk of age (Fig. 7 H).

Once hypertrophic chondrocytes formed at later stages of development, populations of hypertrophic chondrocytes of transgenic mice did not significantly differ from those of normal littermates (Fig. 7, I, J, and M). However, populations of hypertrophic chondrocytes in Smad6 transgenic mice decreased after birth (Fig. 7, K and L). The mean height of zones of hypertrophic chondrocytes was significantly less than that of normal littermates at 3 wk after birth (Fig. 7 N).

Chondrocyte hypertrophy induced by BMP2 was down-regulated in cartilage explants prepared from Smad6 transgenic mice

To investigate BMP signaling in chondrocytes, we organ cultured primordial metatarsal cartilage at 15.0 d.p.c. Phase-contrast microscopy could distinguish the zones of proliferative and mineralized hypertrophic cartilage in the cultures (Fig. 8 A), which was confirmed by histology (Fig. 8, B and C). At the start of culture, metatarsal rudiments from Smad6 transgenic mice were indistinguishable from those of normal mice (Fig. 8, D and E). After 4 d of culture in control medium, the length of hypertrophic cartilage in normal rudiments was increased (Fig. 8 F), whereas transgenic rudiments lacked hypertrophic cartilage (Fig. 8 G). Culture in the presence of rhBMP2 resulted in excessive outgrowth of the proliferative cartilage at both ends of the rudiments and enhanced formation of a hypertrophic center in the normal

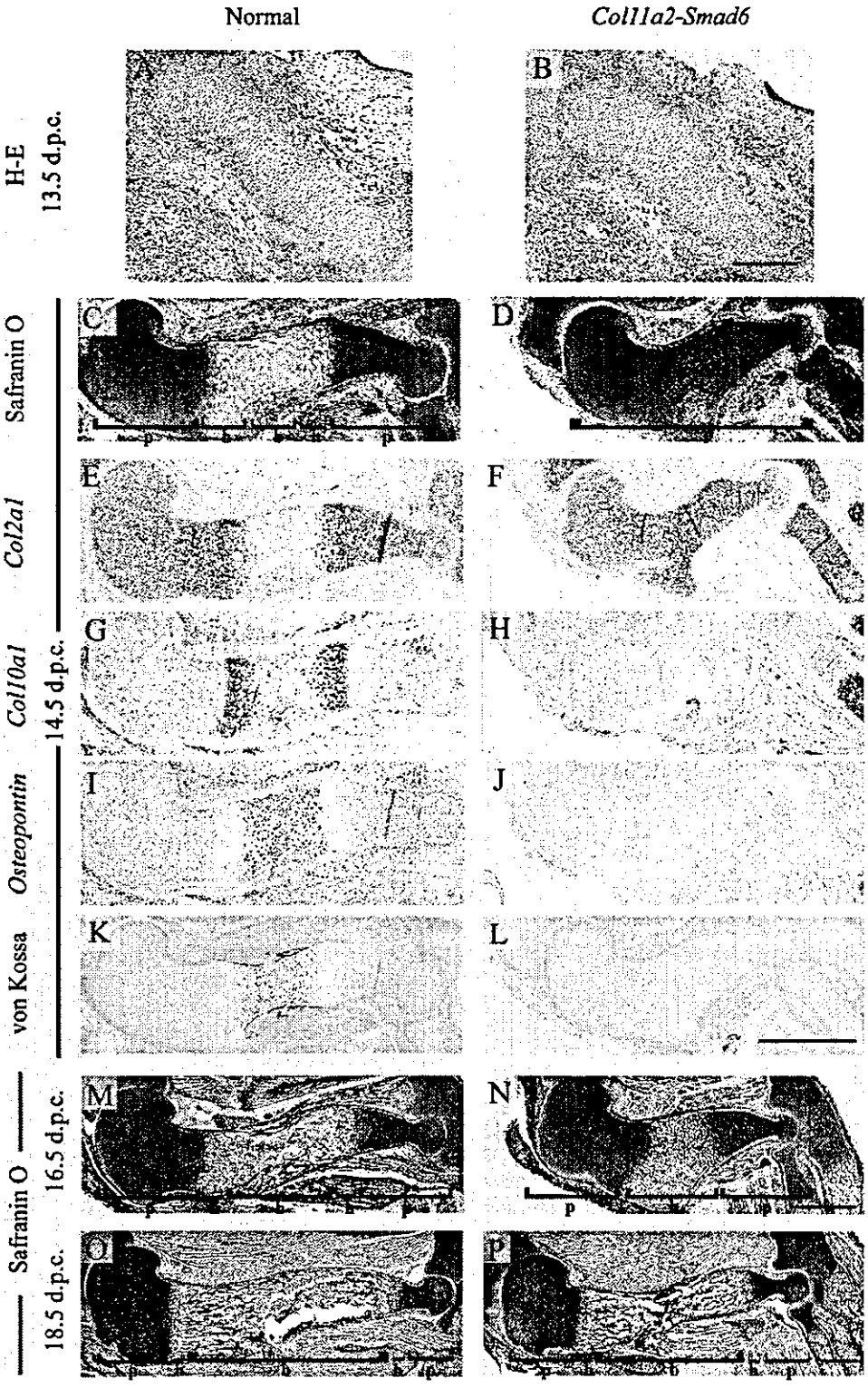

Figure 6. **Delayed hypertrophy of chondrocytes in Smad6 transgenic mice.** Histology of humerus of normal (A, C, E, G, I, K, M, and O) and Smad6 transgenic (B, D, F, H, J, L, N, and P) mice at various stages of development visualized by hematoxylin and eosin (A and B), safranin O/fast green/iron hematoxylin (C, D, and M–P), and von Kossa (K and L) staining. Semi-serial sections to C and D were hybridized with cRNA probes for *Col2a1* (E and F), *Col10a1* (G and H), and osteopontin gene (I and J). p, Proliferative cartilage; h, hypertrophic cartilage; b, bone. Bars: (A and B) 200 μm; (C–P) 500 μm.

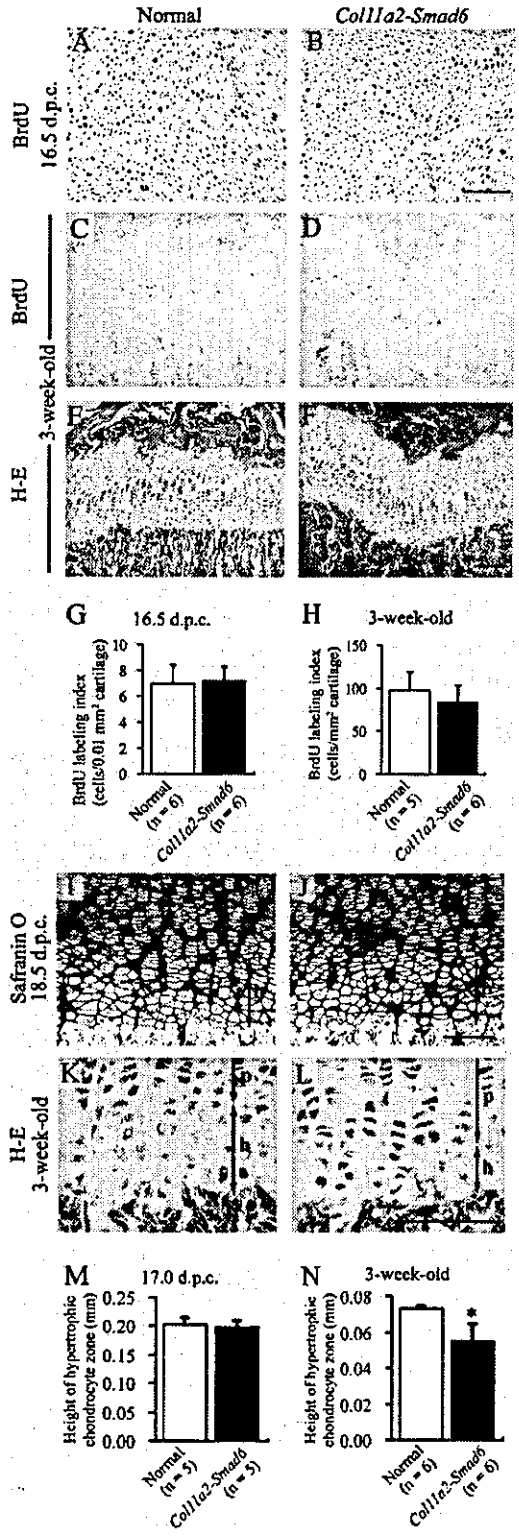

Figure 7. **Normal chondrocyte proliferation and reduced population of hypertrophic chondrocytes in Smad6 transgenic mice.** (A–D) Immunohistochemical detection of BrdU-labeled chondrocytes in proximal humerus. Proliferative chondrocytes of normal (A) and Smad6 transgenic (B) embryos at 16.5 d.p.c.; counterstained with hematoxylin (A and B). Growth plate cartilage of normal (C) and Smad6 transgenic (D) mice at 3 wk of age. (E and F) Serial sections to C and D were stained with hematoxylin and eosin. Numbers of BrdU-positive cells/mm² cartilage compared between normal and transgenic mice at 16.5 d.p.c. (G) and at 3 wk of age (H). (I–L) Zone of hypertrophic chondrocytes of proximal humerus in normal (I and K) and Smad6 transgenic (J and L) mice. Staining with safranin O/fast green/iron hematoxylin at 18.5 d.p.c. (I and J). Staining with hematoxylin and eosin (K and L). Heights of zone of hypertrophic chondrocytes were measured and compared between normal and transgenic mice at 17.0 d.p.c. (M) and at 3 wk of age (N). Error bars show means ± SD. p, Proliferative cartilage; h, hypertrophic cartilage. *, $P < 0.001$ between normal and transgenic mice as determined by *t* test. Bars (A–F and I–L), 100 μm.

rudiments (Fig. 8 H). In transgenic rudiments incubated with rhBMP2, proliferative cartilage expanded (Fig. 8 I) like that of normal mice (Fig. 8 H), but formation of the hypertrophic center was limited (Fig. 8 I) compared with that of normal mice (Fig. 8 H). These findings were confirmed by morphometric analysis of the rudiments (Fig. 8, J and K), indicating that Smad6 overexpression inhibited chondrocyte hypertrophy induced by rhBMP2.

The overexpression of Smurf1 in Smad6/Smurf1 double-transgenic mice enhanced phenotypes of Smad6 transgenic mice

To investigate in vivo function of Smurf1, we generated transgenic mice overexpressing Smurf1 in chondrocytes. We prepared the transgene construct by ligating Smurf1 cDNA with a 5′ FLAG epitope to *Col11a2* promoter/enhancer sequences (*Col11a2-Smurf1*; Fig. 9 A). Smurf1 transgenic mice appeared normal in all respects, as they grew normally after birth and were fertile. Northern blotting demonstrated Smurf1 expression in transgenic limb buds (Fig. 9 B). Transgenic 3-kb Smurf1 mRNA was shorter than endogenous Smurf1 mRNA due to differences at both the 5′ and 3′ untranslated regions. Exogenous rhBMP2 added to Smurf1 transgenic cartilage in organ cultures of metatarsal rudiments at 15.0 d.p.c. caused proliferative cartilage outgrowth and hypertrophic center formation as in normal mice. The mean area of proliferative cartilage in Smurf1 transgenic rudiments (0.44 ± 0.03 mm²) did not significantly differ from that of normal littermates (0.47 ± 0.07 mm²; $n = 6$, $P = 0.08$). The mean length of hypertrophic cartilage in Smurf1 transgenic rudiments (0.26 ± 0.02 mm) also did not significantly differ from that of normal littermates (0.26 ± 0.01 mm; $n = 6$, $P = 0.75$). These results suggest that Smurf1 overexpression does not significantly affect either chondrocyte proliferation or hypertrophy induced by rhBMP2.

We then produced transgenic offspring overexpressing both Smad6 and Smurf1 in chondrocytes (Smad6/Smurf1 double-transgenic mice) by mating Smurf1 transgenic mice with Smad6 transgenic mice of line 199 to test cooperative function of Smad6 and Smurf1. The phenotypes of the double-transgenic mice were similar to but more severe than those of Smad6 transgenic mice. At 16.5 d.p.c., mineralization was evident in the metatarsals of normal and Smurf1 transgenic mice (Fig. 9, C and D, arrowheads), but not in Smad6 transgenic and Smad6/Smurf1 double-transgenic mice (Fig. 9, E and F, arrowheads). The mineralized area in